Synthesis of Novel Group 4 Complexes Bearing the Tropidinyl Ligand: Investigations of Dynamic Behavior, Reactivity, and Catalytic Olefin Polymerization

Steven J. Skoog, Cristina Mateo, Gino G. Lavoie, Frederick J. Hollander, and Robert G. Bergman*

Department of Chemistry, University of California, Berkeley, California 94720

Received January 18, 2000

A new class of group 4 complexes bearing the tropidinyl (Trop) ligand were synthesized. This novel anionic ligand, easily derived from the natural product tropine, is regarded as an analogue of the well-studied Cp ligand (Cp = cyclopentadienyl) and features a bicyclic ring system in which an allyl function donates 4π electrons and an amine function donates 2σ electrons to the metal center. The synthesis of the group 4 complexes involved transmetalation of a stannylated allyl functionality with a group 4 metal halide with concomitant elimination of Me_3SnCl. Reaction of endo-stannylated tropidine (**1**) and $ZrCl_4$, $CpZrCl_3$, or $CpTiCl_3$ afforded the complexes $(Trop)_2ZrCl_2$ (**2**), $(Cp)(Trop)ZrCl_2$ (**3**), and $(Cp)(Trop)TiCl_2$ (**4**), respectively. These dihalide complexes were alkylated using methyllithium to generate $(Trop)_2ZrMe_2$ (**5**), $(Cp)(Trop)ZrMe_2$ (**6**), $(Cp)(Trop)TiMe_2$ (**7**), or benzylmagnesium chloride to give $(Trop)_2ZrBn_2$ (**8**) and $(Cp)(Trop)ZrBn_2$ (**9**). Complexes **2**, **3**, **5**, and **8** were characterized by X-ray crystallography. Complexes **5** and **6** were observed to undergo protonolysis with various acids (HA) to give mixed [Zr]MeA complexes. Reaction of complex **6** with isonitriles (ArNC) gave the η^2-iminoacyl complex (Cp)(Trop)ZrMe[N(Ar)CMe] (**13**), whose structure was confirmed by X-ray crystallography. All the complexes displayed dynamic behavior, and the various exchange processes were investigated by variable-temperature NMR spectroscopy. The dihalide complexes **2**, **3**, and **4** in the presence of modified methylaluminoxane (MMAO) were active catalysts for the polymerization of ethylene. The catalyst system **3**/MMAO displayed a very high ethylene polymerization activity and was similar to that observed for Cp_2ZrCl_2/MMAO. High molecular weight polypropylene was generated using **4**/MMAO, and polypropylene oligomer was obtained using **3**/MMAO. The cationic complex $[(Cp)(Trop)ZrMe][MeB(C_6F_5)_3]$ (**14**) was formed upon reaction of the dimethyl complex **6** with $B(C_6F_5)_3$ and was shown to be an active ethylene polymerization catalyst.

Introduction

When metallocene-based group 4 complexes of type **A** (shown below) are activated with appropriate cocatalysts, they form extremely active olefin polymerization catalysts.[1−3] These are thought to act as "single-site"

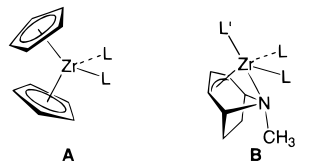

catalysts that generate well-defined polymers from ethylene and other α-olefins. One attractive feature of metallocene catalysts is that they are structurally well defined, with two bent Cp ligands[4] and the L groups forced to lie in a common plane[5] that is commonly referred to as the "wedge". The shape of the wedge is thought to influence the selectivity of the olefin insertion.[6−8] A wide variety of structural modifications have been carried out on this stable framework in order to enhance the polymerization activity and/or selectivity of these catalysts.[9] These include use of so-called "constrained geometry" catalysts to generate isotactic[10] or syndiotactic[11] polypropylene (PP) and nonbridged oscillating metallocene catalysts to make elastomeric stereoblock PP.[12,13]

(1) Kaminski, W. *J. Chem. Soc., Dalton Trans.* **1998**, 1413.
(2) Brintzinger, H. H.; Fischer, D.; Mülhaupt, R.; Reiger, B.; Waymouth, R. M. *Angew. Chem., Int. Ed. Engl.* **1995**, *34*, 1443.
(3) Möhring, P. C.; Coville, N. J. *J. Organomet. Chem.* **1994**, *479*, 1.
(4) Lauher, J. W.; Hoffman, R. *J. Am. Chem. Soc.* **1976**, *98*, 1729.
(5) Albright, T. A.; Burdett, J. K.; Whangbo, M.-H. *Orbital Interactions in Chemistry*; John Wiley & Sons: New York, 1985.
(6) Pino, P.; Cioni, P.; Wei, J. *J. Am. Chem. Soc.* **1987**, *109*, 6189.
(7) Röll, W.; Brintzinger, H. H.; Rieger, B.; Zolk, R. *Angew. Chem., Int. Ed. Engl.* **1990**, *29*, 279.
(8) Erker, G.; Nolte, R.; Aul, R.; Wilker, S.; Krüger, C.; Noe, R. *J. Am. Chem. Soc.* **1991**, *113*, 7594.
(9) Kaminski, W. *Catal. Today* **1994**, *20*, 257.
(10) Kaminski, W.; Külper, K.; Brintzinger, H. H.; Wild, F. R. W. P. *Angew. Chem., Int. Ed. Engl.* **1985**, *24*, 507.
(11) Ewen, J. A.; Elder, M. J.; Jones, R. L.; Haspeslagh, L.; Atwood, J. L.; Bott, S. G.; Robinson, K. *Makromol. Chem., Macromol. Symp.* **1991**, *48/49*, 253.
(12) Coates, G. W.; Waymouth, R. M. *Science* **1995**, *267*, 217.
(13) Hauptman, E.; Waymouth, R. M.; Ziller, J. W. *J. Am. Chem. Soc.* **1995**, *117*, 11586.

10.1021/om000038k CCC: $19.00
Publication on Web 03/09/2000

More recently, attention has been drawn to isoelectronic "nonmetallocene"-based catalysts.[14] In particular, *ansa*-monocyclopentadienylamido group 4 catalysts were found to be highly active polymerization catalysts and are being commercially developed.[15] These new complexes contain metal−nitrogen or metal−oxygen bonds and allow for the generation of polymers with novel microstructures or lead to more robust catalyst systems. Examples of these nonmetallocene group 4 complexes include monoanionic allyl,[16] amidinate,[17−19] amide,[20−26] alkoxy,[27−29] phosphinimide,[30,31] and boratabenzene frameworks,[32−36] macrocyclic,[37,38] tris(pyrazolyl)borate,[39] and oxazoline[40] ligand systems, in addition to dianionic carborane,[41] dienyl,[42,43] and trimethylenemethane[44] ligands.

In a previous communication, we reported the synthesis, reactivity, and olefin polymerization catalysis of zirconium complexes shown above, bearing two tropidinyl (Trop) ligands (**B** where L′ = Trop).[45] This new ligand is isoelectronic to but less symmetric than the Cp ligand and features a split $4\pi + 2\sigma$ electron donor set.[46] The presence of a two-carbon bridge helps to localize the allyl functionality in a specific part of the molecule, and loss of the ligand by β-hydride elimination to form a bridgehead olefin is energetically unfavorable (Bredt's rule).[47−49] In this contribution, we present the synthesis, characterization, reactivity, and catalytic properties of group 4 complexes bearing both one and two Trop ligands.

Scheme 1

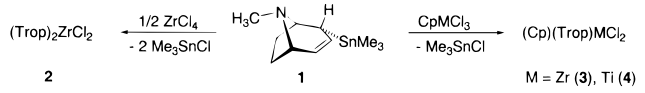

Scheme 2[a]

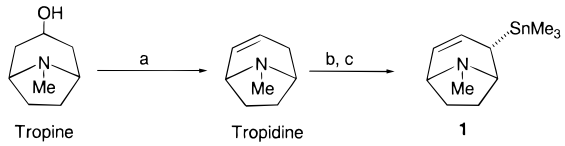

[a] (a) H_2SO_4/AcOH, 160 °C; (b) *t*-BuLi, pentane, < −100 °C; (c) Me_3SnCl, −100 to RT.

Results

Synthesis and Characterization of Tropidinyl-Substituted Metal Halides. The preparation of all dichloride complexes prepared in this study utilized the methodology outlined in Scheme 1. Treatment of the appropriate group 4 metal chloride with the stannylated compound **1** affords the coordinated tropidinyl complex and Me_3SnCl. The tin reagent **1** can be accessed from tropine via tropidine[50] in two steps as previously reported and is illustrated in Scheme 2.[45]

Addition of 2 equiv of **1** to a suspension of $ZrCl_4$ in CH_2Cl_2 at room temperature immediately gave an orange solution of $(Trop)_2ZrCl_2$ (**2**); the complex was isolated in 46% yield (eq 1). Orange crystals were grown

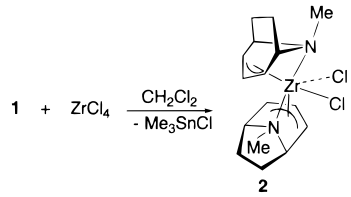

(1)

by slow cooling of a saturated toluene solution, and the solid-state structure was determined by X-ray crystallography. The ORTEP diagram of this complex is shown in Figure 1. Crystal data and selected bond lengths and angles are provided in Tables 1 and 2, respectively. In the solid state **2** has a C_1-symmetric structure in which one Trop ligand is rotated 76.86° with respect to the second. Two different orientations of the Trop ligand with respect to the Cl ligands are observed in this structure. One Trop ligand is bound symmetrically and

(14) Britovsek, G. J. P.; Gibson, V. C.; Wass, D. F. *Angew. Chem., Int. Ed. Engl.* **1999**, *38*, 428.
(15) McKnight, A. L.; Waymouth, R. M. *Chem. Rev.* **1998**, *98*, 2587.
(16) Jiménez Pindado, G.; Thorton-Pett, M.; Bouwkamp, M.; Meetsma, A.; Hessen, B.; Bochmann, M. *Angew. Chem., Int. Ed. Engl.* **1997**, *36*, 2358.
(17) Herkovics-Korine, D.; Eisen, M. S. *J. Organomet. Chem.* **1995**, *503*, 307.
(18) Flores, J. C.; Chien, J. C. W.; Rausch, M. D. *Organometallics* **1995**, *14*, 2106.
(19) Volkis, V.; Shmulinson, M.; Averbuj, C.; Lisovoskii, A.; Edelmann, F. T.; Eisen, M. S. *Organometallics* **1998**, *17*, 3155.
(20) Clark, H. C. S.; Cloke, F. G. N.; Hitchcock, P. B.; Love, J. B.; Wainwright, A. P. *J. Organomet. Chem.* **1995**, *501*, 333.
(21) Scollard, J. D.; McConville, D. H. *J. Am. Chem. Soc.* **1996**, *118*, 10009.
(22) Scollard, J. D.; McConville, D. H.; Payne, N. C.; Vittal, J. J. *Marcomolecules* **1996**, *29*, 5241.
(23) Horton, A. D.; de With, J.; van der Linden, A. J.; van de Weg, H. *Organometallics* **1996**, *15*, 2672.
(24) Warren, T. H.; Schrock, R. R.; Davis, W. M. *Organometallics* **1998**, *17*, 308.
(25) Baumann, R.; Davis, W. M.; Schrock, R. R. *J. Am. Chem. Soc.* **1997**, *119*, 3830.
(26) Gibson, V. C.; Kimberley, B. S.; White, A. J. P.; Williams, D. J.; Howard, P. *Chem. Commun.* **1998**, 313.
(27) van der Linden, A.; Schaverien, C. J.; Meijboom, N.; Ganter, C.; Orpen, A. G. *J. Am. Chem. Soc.* **1995**, *117*, 3008.
(28) Mitani, M.; Oouchi, K.; Hayakawa, M.; Yamada, T.; Mukaiyama, T. *Polym. Bull.* **1995**, *34*, 199.
(29) Fokken, S.; Spaniol, T. P.; Kang, H.-C.; Massa, W.; Okuda, J. *Organometallics* **1996**, *15*, 5069.
(30) Stephan, D. W.; Guérin, F.; Spence, R. E. v. H.; Koch, L.; Gao, X.; Brown, S. J.; Swabey, J. W.; Wang, Q.; Xu, W.; Zoricac, P.; Harrison, D. G. *Organometallics* **1999**, *18*, 2046.
(31) Stephan, D. W.; Stewart, J. C.; Guerin, F.; Spence, R. E. v. H.; Xu, W.; Harrison, D. G. *Organometallics* **1999**, *18*, 1116.
(32) Rogers, J. S.; Lachicotte, R. J.; Bazan, G. C. *J. Am. Chem. Soc.* **1999**, *121*, 1288.
(33) Lee, R. A.; Lachicotte, R. J.; Bazan, G. C. *J. Am. Chem. Soc.* **1998**, *120*, 6037.
(34) Bazan, G. C.; Rodríguez, G.; Ashe, A. J. I.; Al-Ahmad, S.; Kampf, J. W. *Organometallics* **1997**, *16*, 2492.
(35) Rogers, J. S.; Bazan, G. C.; Sperry, C. K. *J. Am. Chem. Soc.* **1997**, *119*, 9305.
(36) Bazan, G. C.; Rodriguez, G.; Ashe, A. J. I.; Al-Ahmad, S.; Müller, C. *J. Am. Chem. Soc.* **1996**, *118*, 2291.
(37) Uhrhammer, D. G.; Black, D. G.; Gardner, T. G.; Olsen, J. D.; Jordan, R. F. *J. Am. Chem. Soc.* **1993**, *115*, 8493.
(38) Martin, A.; Uhrhammer, D. G.; Gardner, T. G.; Jordan, R. F. *Organometallics* **1998**, *17*, 382.
(39) Nakazawa, H.; Irai, S.; Imaoka, K.; Kai, Y.; Yano, T. *J. Mol. Catal.* **1998**, *132*, 33.
(40) Cozzi, P. G.; Gallo, E.; Floriani, C.; Chiesi-Villa, A.; Rizzoli, C. *Organometallics* **1995**, *14*, 4994.
(41) Crowther, D. J.; Baenzinger, N. C.; Jordan, R. F. *J. Am. Chem. Soc.* **1991**, *113*, 1455.
(42) Jiménez-Pindado, G.; Thorton-Pett, M.; Bochmann, M. *J. Chem. Soc., Dalton Trans.* **1997**, 3115.
(43) Hessen, B.; van der Heijden, H. *J. Am. Chem. Soc.* **1996**, *118*, 11670.
(44) Rodríguez, G.; Bazan, G. C. *J. Am. Chem. Soc.* **1995**, *117*, 10155.
(45) Lavoie, G. G.; Bergman, R. G. *Angew. Chem., Int. Ed. Engl.* **1997**, *36*, 2450.
(46) Blümel, J.; Hertkorn, N.; Kanellakopulos, B.; Köhler, F. H.; Lachmann, J.; Müller, G.; Wagner, F. E. *Organometallics* **1993**, *12*, 3896.
(47) Shea, K. J. *Tetrahedron* **1980**, *30*, 1683.
(48) Buchanan, G. L. *Chem. Soc. Rev.* **1974**, *3*, 41.
(49) Köbrich, G. *Angew. Chem., Int. Ed. Engl.* **1973**, *12*, 4.
(50) Ladenburg, A. *Liebigs Ann. Chem.* **1888**, *217*, 118.

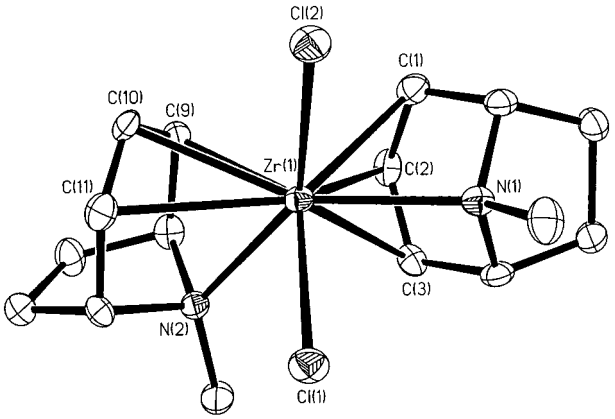

Figure 1. ORTEP diagram of $(Trop)_2ZrCl_2$ (**2**).

bisects the two chlorine atoms in the wedge, while the second Trop ligand is oriented unsymmetrically. The symmetrically bound Trop ligand has similar terminal allyl Zr−C bond distances (Zr−C1 = 2.537(3) Å, Zr−C3 = 2.523(3) Å). The allylic C−C bond distances are nearly identical (C1−C2 = 1.392(4) Å and C2−C3 = 1.400(5) Å). Similar observations were made in structures of metal complexes containing symmetric π-allyl ligands[51] and other types of bicyclic split $4\pi + 2\pi$ electron ligands in late metal systems.[46,52,53] The allylic functionality of the unsymmetrically oriented Trop ligand was more distorted, with the terminal Zr−C and allylic C−C bond distances unequal: Zr−C9 = 2.493(3) Å, Zr−C11 = 2.595(3) Å, C9−C10 = 1.411(4) Å, and C10−C11 = 1.374(4) Å. Similar deviations have been observed in π-allyl complexes in which the chemical environment at one terminal carbon is different from that of the other, due to differing trans-influences.[51] The bond lengths for Zr−Cl(1) and Zr−Cl(2) were found to be 2.5051(8) and 2.5089(8) Å, respectively. These distances are somewhat longer than those reported for zirconocene dichloride (2.44 Å).[54]

The mixed Cp/Trop complex $(Cp)(Trop)ZrCl_2$ (**3**) was synthesized in 81% isolated yield as a mixture of two isomers by adding 1 equiv of **1** to a suspension of $CpZrCl_3$ in CH_2Cl_2 (eq 2 where M = Zr). One of the two

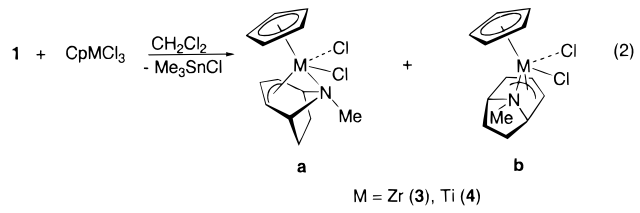

(2)

isomers (**3a**) was isolated as an orange crystalline solid by slow cooling (−30 °C) of a concentrated CH_2Cl_2 solution. The solid-state structure was solved by single-crystal X-ray diffraction. An ORTEP diagram is shown in Figure 2, the crystal data are given in Table 1, and representative bond lengths and angles are given in Table 3. As can be seen from Figure 2, the Trop ligand is oriented symmetrically with respect to the Cl ligands. The molecules in the crystal are located on a crystallographic mirror plane that passes through the zirconium center and bisects both the Cp and Trop ligands. The average Zr−C bond distance for the allyl group is 2.499(8) Å and is similar to the average Zr−C bond distance in zirconocene dichloride (2.49 Å).[54] The Zr−Cp centroid distance was 2.2123(6) Å and is similar to that observed in Cp_2ZrCl_2 (2.20 Å).[54] The Cl−Zr−Cl bond angle is more obtuse (104.45(6)°) than that observed for Cp_2ZrCl_2 (97.1°).[54]

Titanium complex **4** was also synthesized (97% yield) using the methodology illustrated in eq 2 (M = Ti). The ^1H NMR spectra in CD_2Cl_2 at 20 °C exhibited two Cp signals indicating the presence of two isomers **4a** and **4b** in a 5:3 ratio.

Synthesis and Characterization of Dialkyl Complexes. Preparation of the dialkyl complexes was performed by adding 2 equiv of the appropriate organolithium or benzylmagnesium chloride reagent to a suspension of the dichloride complex in Et_2O as shown in eq 3. The products could be isolated by repeated extraction

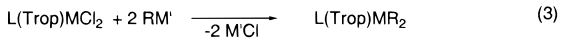

(3)

5 (L = Trop, M = Zr, R = CH_3, M' = Li)
6 (L = Cp, M = Zr, R = CH_3, M' = Li)
7 (L = Cp, M = Ti, R = CH_3, M' = Li)
8 (L = Trop, M = Zr, R = $CH_2C_6H_5$, M' = MgCl)
9 (L = Cp, M = Zr, R = $CH_2C_6H_5$, M' = MgCl)

with hydrocarbon solvents and subsequent crystallization at −30 °C. The dimethylzirconium complexes were observed to decompose under prolonged dynamic vacuum, so care was taken to avoid extended exposure of these materials to vacuum in the solid state. Similar observations were made with $(Cp)_2TiMe_2$.[55−57]

The dimethyl complex $(Trop)_2ZrMe_2$ (**5**) was characterized by X-ray crystallography and shown to have a structure similar to that of $(Trop)_2ZrCl_2$ (**2**); the crystal data and selected bond distances and angles are given in Tables 1 and 4, respectively using the same numbering scheme as for **2**.[58] The Trop ligands feature two different orientations (symmetric and unsymmetric with respect to the CH_3 ligands) and are rotated with respect to one another by 87.71°, more than 10° greater than in **2**. The average Zr−C bond distance (2.562(5) Å) and the average Zr−N distance (2.384(3) Å) are longer than those observed in complexes **2** or **3**. The average Zr−Me bond length is 2.315(3) Å and is longer than the average Zr−Me distance measured for Cp_2ZrMe_2 (2.276(7) Å).[59] The corresponding Me−Zr−Me bond angle is 98.75(9)°, which is larger than that reported for dimethylzirconocene (95.6(12)°).[59]

The dibenzyl complex $(Trop)_2ZrBn_2$ (**8**) was characterized by X-ray crystallography. An ORTEP diagram is

(51) Clarke, H. L. *J. Organomet. Chem.* **1974**, *80*, 155.
(52) Blümel, J.; Köhler, F. H.; Müller, G. *J. Am. Chem. Soc.* **1988**, *110*, 4846.
(53) Blümel, J.; Köhler, F. H.; Müller, G.; Wilkenson, D. L. *Angew. Chem., Int. Ed. Engl.* **1988**, *27*, 977.
(54) Prout, K.; Cameron, T. S.; Forder, R. A.; Critchley, S. R.; Denton, B.; Rees, G. V. *Acta Crystallogr., Sect. B* **1974**, *30*, 2290.
(55) Herrmann, W. A.; Salzer, A. *Synthetic Methods of Organometallic and Inorganic Chemistry*; Theim Medical Publishers: New York, 1996; pp 92−93.
(56) Erskine, G. J.; Hartgerink, J.; Weinberg, E. L.; McCowan, J. D. *J. Organomet. Chem.* **1979**, *170*, 51.
(57) Alt, H. G.; Di Sanzo, F. P.; Rausch, M. D.; Uden, P. C. *J. Organomet. Chem.* **1976**, *107*, 257.
(58) The details of the structure determination, an ORTEP diagram, and complete tables containing the crystal data, bond distances, bond angles, and positional and thermal displacement parameters are given in the Supporting Information.
(59) Hunter, W. E.; Hrncir, D. C.; Bynum, R. V.; Penttila, R. A.; Atwood, J. L. *Organometallics* **1983**, *2*, 750.

Table 1. Summary of Crystallographic Data for 2, 3, 5, 8, and 13

	2	3	5	8	13
cryst syst	monoclinic	orthorhombic	monoclinic	monoclinic	monoclinic
cryst color, habit	orange, plate	orange, column	yellow, tabular	yellow, tabular	colorless, prismatic
space group	$P2_1/n$ (#14)	*Pnma* (#62)	$P2_1/c$(#14)	$P2_1/c$ (#14)	$P2_1/c$ (#14)
formula	$C_{16}H_{24}Cl_2N_2Zr$	$C_{13}H_{17}Cl_2NZr$	$C_{18}H_{26}N_2Zr$	$C_{30}H_{36}N_2Zr$	$C_{24}H_{32}N_2Zr$
MW, g mol^{-1}	406.51	349.41	361.64	517.86	439.75
a, Å	7.0931(2)	13.0007(7)	7.1659(1)	7.6088(1)	7.8640(3)
b, Å	18.2744.2	10.8353(6)	15.1415(1)	16.5441(2)	21.9650(7)
c, Å	12.8139(3)	9.6386(5)	15.8990(2)	20.1281(2)	12.6845(4)
β, deg	95.777(1)		90.998(1)	99.943(1)	106.124(1)
V, Å^3	1652.53(5)	1357.76(11)	1724.82(3)	2495.68(5)	2104.84(11)
Z	4	4	4	4	4
ρ(calcd), g cm^{-3}	1.634	1.709	1.393	1.378	1.388
temp, °C	−120	−107	−124	−127	−101
R	0.028	0.029	0.023	0.026	0.028
R_w	0.035	0.030	0.035	0.035	0.036
R_{all}	0.042	0.061	0.029	0.037	0.037
goodness of fit	1.33	1.20	1.47	1.43	1.68

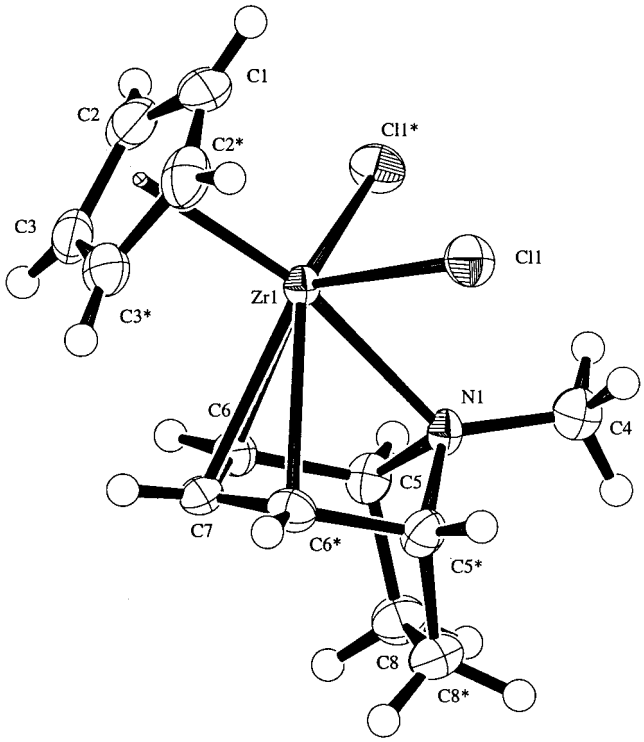

Figure 2. ORTEP diagram of (Cp)(Trop)$ZrCl_2$ (**3**).

Table 2. Selected Bond Distances (Å) and Bond Angles (deg) of $(Trop)_2ZrCl_2$ (2)

Zr−Cl1	2.5051(8)	Zr−N1	2.352(3)
Zr−Cl2	2.5089(8)	Zr−N2	2.369(3)
Zr−C1	2.537(3)	Zr−C9	2.493(3)
Zr−C2	2.518(3)	Zr−C10	2.532(3)
Zr−C3	2.523(3)	Zr−C11	2.595(3)
C1−C2	1.392(4)	C9−C10	1.411(4)
C2−C3	1.400(5)	C10−C11	1.374(4)
Cl1−Zr−Cl2	100.89(3)	N1−Zr−N2	133.01(9)
C7−C1−C2	116.2(3)	C15−C9−C10	115.6(3)
C4−C3−C2	116.4(3)	C12−C11−C10	117.1(3)
C1−C2−C3	119.8(3)	C9−C10−C11	120.2(3)

shown in Figure 3, the crystal data are presented in Table 1, and selected bond distances and angles are given in Table 5. The C17−Zr−C24 bond angle is 87.91-(8)° and is smaller than the Me−Zr−Me angle in **5**. One Trop ligand has the allyl function directed toward C24, while the other Trop ligand has a nitrogen directed toward C17. This could be due to a steric effect in which the Trop ligands are directed away from the wedge by

Table 3. Selected Bond Distances (Å) and Bond Angles (deg) of (Cp)(Trop)$ZrCl_2$ (3)

Zr−C1	2.504(7)	Zr−C6	2.493(5)
Zr−C2	2.528(5)	Zr−C7	2.506(7)
Zr−C3	2.497(4)	Zr−N1	2.333(5)
Zr−Cp	2.2123(6)	Zr−Cl1	2.4705(11)
		C6−C7	1.392(5)
Cl1−Zr−Cl1*	104.45(6)	Zr−N1−C4	128.0(4)
Cp−Zr−Cl1	105.51(3)	C4−N1−C5	113.7(5)
Cl1−Zr−C7	119.84(7)	C5−N1−C5*	100.7(5)
C1−C2−C3	107.7(5)	C5−C6−C7	115.4(5)
C2−C1−C2*	108.8(7)	C6−C7−C6*	120.1(6)
C2−C3−C3*	107.8(3)		

Table 4. Selected Bond Distances (Å) and Bond Angles (deg) of $(Trop)_2ZrMe_2$ (5)

Zr−C17	2.316(2)	Zr−N1	2.389(2)
Zr−C18	2.315(2)	Zr−N2	2.379(2)
Zr−C1	2.685(2)	Zr−C9	2.504(2)
Zr−C2	2.553(2)	Zr−C10	2.549(2)
Zr−C3	2.437(2)	Zr−C11	2.647(2)
N1−C8	1.472(3)	N2−C16	1.465(3)
C17−Zr−C18	98.75(9)	N1−Zr−N2	129.45(6)
C7−C1−C2	117.0(2)	C15−C9−C10	115.5(2)
C4−C3−C2	114.2(2)	C12−C11−C10	116.4(2)
C1−C2−C3	120.8(2)	C9−C10−C11	120.8(2)
C4−N1−C7	100.3(2)	C12−N2−C15	100.8(2)
Zr−N1−C8	128.7(1)	Zr−N2−C16	126.3(1)

the bulky aryl groups. The ^{1}H NMR spectra of **8** in C_6D_6 at room temperature were consistent with an averaged structure of C_{2v} symmetry (Table 6), and a single resonance was observed for the benzylic protons.

The ^{1}H NMR spectrum of the dibenzylzirconium complex (Cp)(Trop)$ZrBn_2$ (**9**) at 25 °C was consistent with a complex exhibiting C_s symmetry (Table 6). The benzylic protons were observed to be diastereotopic, and two sharp doublets were observed at 2.07 and 1.83 ppm with $^1J_{Ha-Hb}$ = 10.5 Hz at ambient temperature and consistent with the structure shown below.

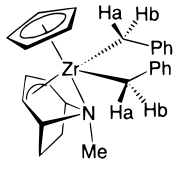

9

Dynamic Behavior of Group 4 Complexes. Analysis of the ^{1}H NMR spectrum of **2** in CD_2Cl_2 at room temperature reveals a simple pattern consistent with

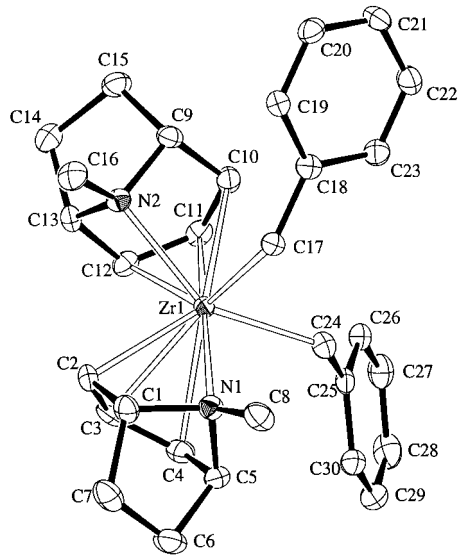

Figure 3. ORTEP diagram of $(Trop)_2ZrBn_2$ (**8**).

Table 5. Selected Bond Distances (Å) and Bond Angles (deg) of $(Trop)_2ZrBn_2$ (8)

Zr−C17	2.356(2)	Zr−N1	2.396(2)
Zr−C24	2.378(2)	Zr−N2	2.375(2)
Zr−C2	2.470(2)	Zr−C10	2.570(2)
Zr−C3	2.535(2)	Zr−C11	2.521(2)
Zr−C4	2.588(2)	Zr−C12	2.530(2)
C17−C18	1.476(3)	C24−C25	1.475(3)
C17−Zr−C24	87.91(8)	N1−Zr−N2	124.3(7)
C1−C2−C3	115.1(2)	C9−C10−C11	115.7(2)
C5−C4−C3	117.1(2)	C13−C12−C11	116.9(2)
C2−C3−C4	119.6(2)	C10−C11−C12	120.3(2)
C1−N1−C5	100.4(2)	C9−N2−C13	101.0(2)
Zr−N1−C8	135.5(1)	Zr−N2−C16	126.6(1)
Zr−C17−C18	128.9(2)	Zr−C24−C25	132.5(2)

C_{2v} symmetry (Table 6). Upon cooling a CD_2Cl_2 solution of **2**, the three allylic and two bridgehead resonances broadened and separated into 10 signals, all integrating to the same area at −90 °C (Figure 4). The coalescence temperature for the central allylic resonances was −48 °C, and the peak separation ($\delta\nu$) of these two resonances at −90 °C was 168 Hz. The rate, calculated using eq 4,

$$k = \pi\delta\nu/\sqrt{2} \qquad (4)$$

at the coalescence temperature for an equally populated two-site exchange[60] is given in Table 7 along with the corresponding activation barrier.[61]

Complexes **3** and **4** were isolated as a mixture of two isomers; the major isomer exhibits apparent C_s symmetry (**3a** and **4a**), and the minor isomer exhibits C_1 symmetry (**3b** and **4b**) (Table 6). The relative concentration of the different isomers was observed to change as a function of temperature (Table 8). A van't Hoff plot is shown in Figure 5; for complex **3** $\Delta H° = 0.8 \pm 0.1$ kcal mol^{-1}, and $\Delta S° = 1.2 \pm 0.4$ cal mol^{-1} K^{-1}; for complex **4** $\Delta H° = -0.75 \pm 0.06$ kcal mol^{-1}, and $\Delta S° = 3.5 \pm 0.2$ cal mol^{-1} K^{-1}.

The assignments of the allyl and bridgehead resonances for **4b** given in Table 6 were made with the aid of 2D EXSY ^{1}H NMR spectroscopy and extrapolated to **3b**. The cross-peaks between resonances corresponding to **4a** (where the allylic and bridgehead resonances were known) and **4b** were used to make the assignments. The 2D EXSY ^{1}H NMR spectrum of **4** using a mixing time of 7 s, along with the relevant assignments, is given in the Supporting Information.

The rate of exchange between **3a** and **3b** was calculated from the line width at half-height of the Cp resonance (W = 12 Hz) at 20 °C (the fast exchange region) using eq 5[60,62] where p_a and p_b are the populations of **3a** and **3b**, respectively, W_o is the line width at half-height in the absence of exchange (3 Hz), and $\delta\nu$ = 120 Hz. The rate and the corresponding activation barrier are given in Table 7. For **4a** and **4b**, upon heating in $C_2D_2Cl_4$, the two Cp resonances broadened and coalesced at 70 °C. At 100 °C a broadened spectrum exhibiting apparent C_s symmetry was finally observed (Table 6). The rate of interconversion was calculated using eq 5 and the two different Cp resonances (W = 42 Hz at 70 °C, $\delta\nu$ = 99 Hz).[60] The rate and activation barrier[61] for this process are given in Table 7.

$$k_1 = 4\pi p_a p_b{}^2 \delta\nu^2/(W - W_o) \qquad (5)$$

At room temperature the ^{1}H NMR spectrum of the dialkyl complexes **5**, **6**, **7**, and **9** was consistent with a symmetric complex (Table 6). No extensive broadening of any resonance was observed for complexes **6** and **9** upon cooling in CD_2Cl_2. However, upon cooling a CD_2Cl_2 solution of **5**, the resonances in the allylic and bridgehead region of the ^{1}H NMR spectrum began to broaden at −60 °C, and decoalesence of the central allyl signal was observed at −95 °C. A spectrum at the slow exchange limit for this complex was not observed, prohibiting calculation of the activation barrier for this process. Upon cooling a CD_2Cl_2 sample of **7**, the single TiMe resonance began to broaden, and decoalesence was observed at −40 °C. Two separate TiMe resonances were finally observed at −80 °C (Figure 6). The low-temperature ^{1}H NMR spectrum was consistent with a complex of C_1 symmetry. The rate for this exchange process (averaging of the different Trop and TiMe resonances) was calculated at the coalescence temperature of the two TiMe resonances based on the separation observed at the slow exchange limit ($\delta\nu$ = 414 Hz at −90 °C) using eq 4.[60] The rate is reported in Table 7 along with the corresponding activation barrier.[61]

Reactivity of Tropidinyl(dimethyl)zirconium Complexes with Proton Donors. Protonolysis of complex **5** with *tert*-butyl alcohol at room temperature gave $(Trop)_2Zr(Me)(O\text{-}t\text{-}Bu)$, **10** (88% yield), and 1 equiv of methane (Scheme 3). Protonolysis of complex **5** with 1 equiv of trifluoromethanesulfonic acid formed $(Trop)_2Zr(Me)(OSO_2CF_3)$ (**11**) and 1 equiv of methane. This compound could be easily generated but was found to undergo slight decomposition during the purification process, prohibiting satisfactory elemental analysis. Addition of KO-*t*-Bu to **11** gave $(Trop)_2Zr(Me)(O\text{-}t\text{-}Bu)$ (**10**) that was substantially more stable (89% yield). Addition of 1 equiv of LiNH-*t*-Bu to **11** gave $(Trop)_2Zr(Me)(NH\text{-}t\text{-}Bu)$ (**12**). This complex was also spectroscopically characterized, but lacked sufficient stability to allow adequate purification for microanalysis. These

(60) Binsch, G. In *Band-Shape Analysis*; Jackman, L. M., Cotton, F. A., Eds.; Academic Press: New York, 1975; pp 45−81.
(61) Sandström, J. *Dynamic NMR Spectroscopy*; Academic Press: London, 1982; pp 77−92.
(62) Petit, L. H.; Anderson, W. A. *J. Chem. Phys.* **1959**, *30*, 899.

Table 6. ^{1}H NMR Spectroscopic Data for Trop-Bearing Complexes[a]

	elevated-temperature spectrum					low-temperature spectrum				
compd	δ(ppm)	mult	*J* (Hz)	int	assgnt	δ(ppm)	mult	*J* (Hz)	int	assgnt
$(Trop)_2ZrCl_2$[b] (**2**)	5.72	t	7	2	central allylic	6.04	t	7	1	central allyl
	4.29	q	7, 2	4	terminal allylic	5.47	t	7	1	central allyl
	3.73	br		4	bridgehead	4.55	br		1	terminal allylic
	2.48	s		6	NMe	4.30	br		1	terminal allylic
	2.23	s		8	CH_2	4.28	br		1	*c*
						4.11	br		1	*c*
						4.02	br		1	*c*
						3.88	br		1	bridgehead
						3.72	br		1	bridgehead
						2.89	br		1	bridgehead
						2.51	s		3	NMe
						2.18	s		3	NMe
						2.2−1.98	m		8	CH_2
(Cp)(Trop)$ZrCl_2$[d] (**3**)						6.20	s		5	Cp
						5.65	t	7	1	central allylic
						4.37	q	7, 4.5	2	terminal allylic
						3.77	br		2	bridgehead
	6.21	s		5	Cp	2.12	s		3	NMe
	5.64	br		1	central allylic	2.2−2.09	m		4	CH_2
	4.37	br		2	terminal allylic					
	3.81	br		2	bridgehead	6.60	s		5	Cp
	2.59	s		3	NMe	5.90	t	7	1	central allylic
	2.20	br		4	CH_2	5.07	m		1	terminal allylic
						3.09	m		1	terminal allylic
						3.28	br		1	bridgehead
						2.76	br		1	bridgehead
						2.5	s		3	NMe
						2.2−2.09	m		4	CH_2
(Cp)(Trop)$TiCl_2$[e] (**4**)						6.32	s		5	Cp
						5.08	t	7.2	1	central allylic
						4.77	q	7, 4.9	2	terminal allylic
						4.16	br		2	bridgehead
	5.8	br		5	Cp	2.88	s		3	NMe
	4.6	br		1	central allylic	2.22−1.79	m		4	CH_2
	4.1	br		2	terminal allylic					
	3.6	br		2	bridgehead	6.65	s		5	Cp
	2.1	br		3	NMe	5.89	t	5.9	1	terminal allylic
	1.6	br		2	CH_2	5.62	t	7.5	1	central allylic
	1.4	br		2	CH_2	4.44	t	4.8	1	terminal allylic
						4.32	br		1	bridgehead
						3.17	br		1	bridgehead
						2.88	s		3	NMe
						2.22−1.79	m		4	CH_2
$(Trop)_2ZrMe_2$[f] (**5**)	4.86	t	7.4	2	central allylic	*g*				
	3.87	q	7.3	4	terminal allylic					
	3.31	br		4	bridgehead					
	2.12	m		4	CH_2					
	2.02	m		3	NMe					
	1.90	m		4	CH_2					
	0.22	s		6	ZrMe					
(Cp)(Trop)$ZrMe_2$[h] (**6**)	5.77	s		5	Cp	*i*				
	4.34	t	7.5	1	central allylic					
	3.84	q	7.2, 4.5	2	terminal allylic					
	3.18	br		2	bridgehead					
	1.99	q	10.2, 4.5	2	CH_2					
	1.86	s		3	NMe					
	1.78−1.72	m		2	CH_2					
	0.08	s		6	ZrMe					
(Cp)(Trop)$TiMe_2$[j] (**7**)	6.24	s		5	Cp	6.25	s		5	Cp
	5.08	t	10	1	central allylic	5.46	br		1	terminal allylic
	4.60	br		2	terminal allylic	5.04	t	7.5	1	central allylic
	3.24	br		2	bridgehead	3.94	br		1	terminal allylic
	2.23	q	15, 5	2	CH_2	3.75	br		1	bridgehead
	2.11	m		2	CH_2	2.31	br		1	bridgehead
	1.65	s		2	NMe	2.18	br		2	CH_2
	−0.2			6	TiMe	1.90	m		2	CH_2
						1.53	s		3	NMe
						0.07	s		3	TiMe
						−1.31	s		3	TiMe
$(Trop)_2ZrBn_2$[k] (**8**)	5.14	t	7.4	2	central allylic					
	3.79	q	7.5, 4.5	4	terminal allylic					
	2.85	br		4	bridgehead					
	2.05	s		6	NMe					

Table 6 (Continued)

compd	elevated-temperature spectrum δ(ppm)	mult	J (Hz)	int	assgnt	low-temperature spectrum δ(ppm)	mult	J (Hz)	int	assgnt
$(Trop)_2ZrBn_2$[k] (**8**)	1.95	s		4	$ZrCH_2$					
	1.72	s		8	CH_2					
	7.27	t	7.7	4	Ar					
	7.12	t	7.7	4	Ar					
	6.90	t	7.7	2	Ar					
(Cp)(Trop)$ZrBn_2$[l] (**9**)	5.77	s		5	Cp	*m*				
	4.54	t	7.5	1	central allylic					
	3.76	t	5.7	2	terminal allylic					
	2.96	br		2	bridgehead					
	2.07	d	10.4	2	$ZrCH_2$					
	1.88	d	7.4	2	CH_2					
	1.83	d	10.4	2	$ZrCH_2$					
	1.65	m		5	NMe, CH_2					

[a] Spectrum collected at 300 MHz. [b] In CD_2Cl_2 at 20 and −90 °C. [c] Bridgehead or allyl resonance. [d] In CD_2Cl_2 at 20 and −70 °C. [e] In $C_2D_2Cl_4$ at 100 °C and $CDCl_3$ at 20 °C. [f] In CD_2Cl_2 at 20 °C. [g] Only exchange-broadened peaks observed at −95 °C. [h] In CD_2Cl_2 at 20 °C. [i] No appreciable broadening observed at −95 °C in CD_2Cl_2. [j] In CD_2Cl_2 at 20 and −90 °C. [k] In C_6D_6 at 20 °C. [l] In C_6D_6 at 20 °C. [m] No appreciable broadening observed at −78 °C in CD_2Cl_2.

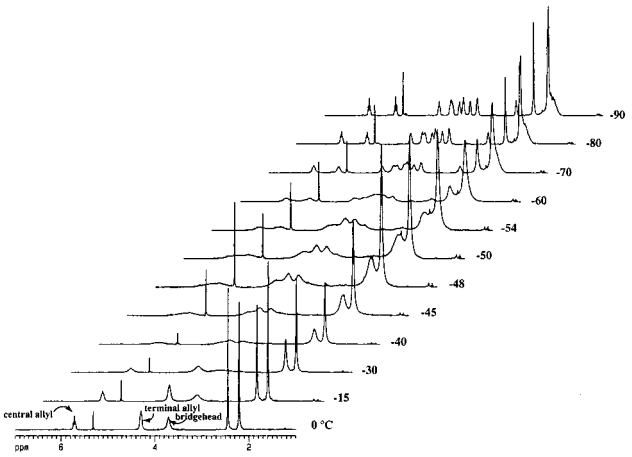

Figure 4. Variable-temperature ^1H NMR spectra of $(Trop)_2ZrCl_2$ (**2**) in CD_2Cl_2.

Table 7. Rates and Free Energies of Activation for the Solution Dynamic Processes of Group 4 Complexes Bearing the Trop Ligand

complex	T (°C)	k_1 (s^{-1})	$\Delta G^{\ddagger}$ (kcal mol^{-1})	K
(Cp)(Trop)$Ti(CH_3)_2$[a]	−40[b]	1191 ± 6[c]	10.2 ± 0.1	1
$(Trop)_2ZrCl_2$[a]	−48[b]	373 ± 5[c]	10.9 ± 0.1	1
(Cp)(Trop)$ZrCl_2$[a]	20	324 ± 180[d]	13.8 ± 0.3	0.13 ± 0.06[e]
(Cp)(Trop)$TiCl_2$[f]	70	592 ± 150[d]	15.8 ± 0.2	0.50 ± 0.07[e]

[a] Spectrum collected in CD_2Cl_2. [b] Coalescence temperature. [c] Rate calculated for degenerate exchange using eq 4. [d] Rate for eq 11 calculated using eq 5. [e] Value extrapolated from van't Hoff plot. [f] Spectrum collected in $C_2D_2Cl_4$.

mixed complexes each exhibited five-signal patterns in the bridgehead and allylic region of the ^1H NMR spectra that are characteristic of Trop complexes with apparent C_1 symmetry. Treatment of the dimethylzirconium complex **6** in C_6D_6 with 10 equiv of the trialkylammonium hydrochloride salt $(n\text{-}Bu)_3NHCl$ led to the immediate formation of **3** in an 87% yield by NMR relative to an internal standard (eq 6).

$$\underset{\mathbf{6}}{(Cp)(Trop)ZrMe_2} + \text{excess } (n\text{-}Bu)_3NHCl \xrightarrow[-2\ CH_4]{C_6D_6} \underset{\mathbf{3}}{(Cp)(Trop)ZrCl_2} + 2\ n\text{-}Bu_3N \quad (6)$$

Insertion Chemistry of Isonitriles with (Cp)(Trop)$ZrMe_2$ (5). To explore the migratory insertion behavior of tropidinyl complexes, the reactions of **6** with isonitriles and CO were investigated. Reaction of 2,6-$Me_2C_6H_3NC$ with complex **6** was found to readily form the η^2-iminoacyl **13** (eq 7). Insertion products were also observed using *t*-BuNC, but treatment with CO led only

Table 8. Equilibrium Data for Group 4 Complexes Bearing the Trop Ligand[a]

complex	T (°C)	K
(Cp)(Trop)$TiCl_2$ (**4**)	48	0.55 ± 0.01
	36	0.57 ± 0.01
	27	0.59 ± 0.02
	19	0.60 ± 0.02
	13	0.61 ± 0.02
(Cp)(Trop)$ZrCl_2$ (**3**)	0	0.11 ± 0.01
	−30	0.099 ± 0.01
	−50	0.088 ± 0.008
	−70	0.065 ± 0.006

[a] Equilibrium for the conversion of **a** to **b** (eq 11).

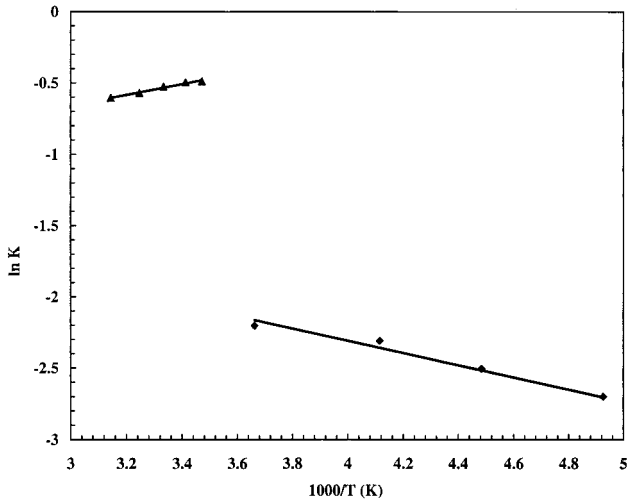

Figure 5. A van't Hoff plot for the equilibration between the symmetric (**a**) and nonsymmetric (**b**) isomers (eq 11) of (Cp)(Trop)MCl_2 **3** and **4** where M = Ti (▲) and Zr (◆), respectively.

$$\underset{\mathbf{6}}{(Cp)(Trop)ZrMe_2} + \text{CN-}(2,6\text{-}Me_2C_6H_3) \longrightarrow \underset{\mathbf{13}}{(Cp)(Trop)Zr(\eta^2\text{-}C(=N\text{-}2,6\text{-}Me_2C_6H_3)Me)} \quad (7)$$

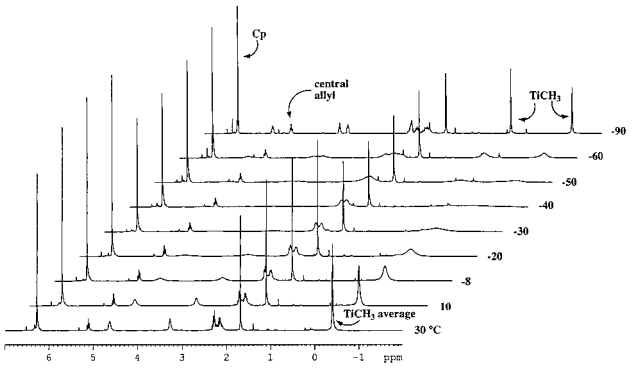

Figure 6. Variable-temperature ^{1}H NMR spectra of (Cp)(Trop)Ti(CH_3)$_2$ (**7**) in CD_2Cl_2.

Scheme 3

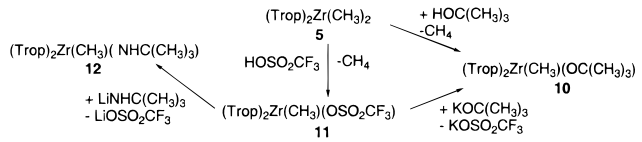

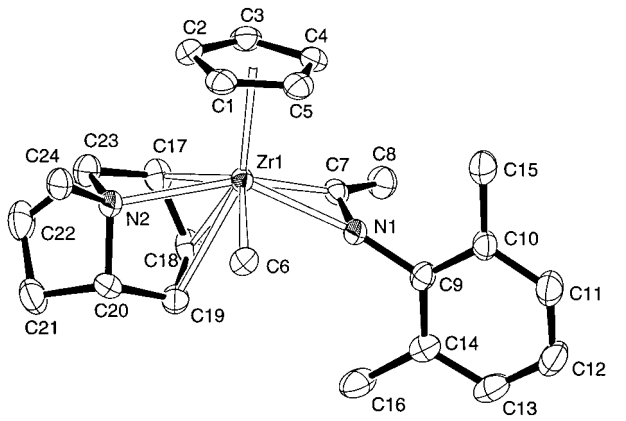

Figure 7. ORTEP diagram of(Cp)(Trop)Zr(CH_3)[N(2,6-(CH_3)$_2$$C_6H_3$)C($CH_3$)] (**13**).

to unidentified decomposition products. The aminoacyl methyl resonance for **13** was observed at 1.78 ppm, and the ^{13}C{^{1}H} NMR chemical shift of the aminoacyl carbon at 247.6 ppm was consistent with those of other aminoacyl complexes.[63−66] The infrared spectrum revealed a ν_{CN} stretch at 1577 cm^{-1}, consistent with η^2-coordination of the iminoacyl ligand.[64] Complex **13** was crystallized as colorless blocks and characterized by X-ray crystallography. An ORTEP diagram is given in Figure 7; crystal data and selected bond distances and angles are given in Tables 1 and 9, respectively. The imino carbon atom is bound directly to the zirconium atom, and the Zr−C7 bond length (2.238(3) Å) is similar to Zr−C(iminoacyl) bond distances observed in other complexes (2.23−2.25 Å).[63,67] The Zr−Cp(centroid) distance (2.2612(2) Å) is similar to that observed in CpCp*Zr-[C(N-2,6$Me_2C_6H_3$)Si($SiMe_3$)]Cl (2.254(11) Å).[64] The bond

Table 9. Selected Bond Distances (Å) and Bond Angles (deg) of (Cp)(Trop)Zr(CH_3)[N(2,6-(CH_3)$_2$$C_6H_2$)C($CH_3$)] (13)

Zr−C1	2.559(3)	Zr−C17	2.485(3)
Zr−C2	2.574(3)	Zr−C18	2.529(3)
Zr−C3	2.554(3)	Zr−C19	2.6512(3)
Zr−C4	2.551(3)	Zr−C6	2.346(3)
Zr−C5	2.550(3)	Zr−C7	2.238(3)
Zr−Cp	2.2612(2)	C7−C8	1.498(4)
Zr−N2	2.402(2)	C7−N1	1.275(3)
Zr−N1	2.277(2)	N1−C9	1.452(3)
Cp−Zr−C6	106.57(6)	N1−Zr−C7	32.79(8)
Cp−Zr−C7	104.35(6)	Zr−C7−N1	75.32(17)
Cp−Zr−N1	111.00(5)	Zr−N1−C7	71.89(15)
C6−Zr−N1	83.44(8)	Zr−N1−C9	162.54(17)
C17−C18−C19	121.5(3)	Zr−C7−C8	159.7(2)
C18−C17−C23	114.0(3)	C6−Zr−C7	115.78(9)
C18−C19−C20	116.6(3)		

angles of the triangle defined by Zr−C7−N1 are similar to those of other structurally characterized η^2-iminoacyl complexes[63,64] as well as the η^2-silaacyl complex Cp_2Zr-(η^2-C(O)$SiMe_3$)Cl.[65,68] The Trop ligand adopts a nonsymmetrical orientation with respect to the wedge. The coordination of the allyl group was also irregular, where the Zr−C19 bond distance (2.6512(3) Å) is much larger than that of the Zr−C17 bond distance (2.485(3) Å), possibly due to steric crowding with the methyl (C16) of the 2,6-dimethylphenyl ring.

Ethylene Polymerization. The ethylene polymerization activities for the group 4 complexes used in this study were measured at 25 °C in toluene using 1000 equiv of modified methylaluminoxane (MMAO) under 1 atm of ethylene (Table 10).[69] Polyethylene (PE) molecular weights were determined by gel permeation chromatography (GPC), and melting points were determined by differential scanning calorimetry (DSC). The **3**/MMAO system is very active[14] (9.86×10^6 g PE mol [M]$^{-1}$ h^{-1} atm^{-1}), exhibiting a rate and polydispersity of PE similar to that observed with Cp_2ZrCl_2/MMAO (control experiments run using Cp_2ZrCl_2/MMAO were consistent with previous reports in the literature).[70−72] The use of the borane cocatalyst tris(pentafluorophenyl)-borane ($B(C_6F_5)_3$) with **6** resulted in slightly lower activity relative to **3**/MMAO (Table 10). The other Trop-bearing complexes (**2** and **4**) displayed only moderate polymerization activity under these conditions.

High-density PE was produced from all the catalyst systems with the exception of **4**/MMAO and $CpZrCl_3$/MMAO, as evidenced by the high melting points of the produced PE.[73] Polymerizations carried out with $CpZrCl_3$/MMAO, $CpTiCl_3$/MMAO, and $ZrCl_4$/MMAO gave very low activities. Two distinct melting endotherms were detected by DSC for polymers produced using the $CpTiCl_3$/MMAO and $ZrCl_4$/MMAO systems.

The catalyst activity as a function of time was investigated by measuring the ethylene uptake of the

(63) Chamberlain, L. R.; Durfee, L. D.; Fanwick, P. E.; Kobriger, L.; Latesky, S. L.; McMullen, A. K.; Rothwell, I. P.; Folting, K.; Huffman, J. C.; Streib, W. E.; Wang, R. *J. Am. Chem. Soc.* **1997**, *109*, 3390.
(64) Elsner, F. H.; Tilley, T. D.; Rheingold, A. L.; Geib, S. J. *J. Organomet. Chem.* **1987**, *358*, 169.
(65) Campion, B. K.; Falk, J.; Tilley, T. D. *J. Am. Chem. Soc.* **1987**, *109*, 2049.
(66) Wolczanski, P. T.; Bercaw, J. E. *J. Am. Chem. Soc.* **1979**, *101*, 6450.
(67) Cardin, D. J.; Lappert, M. F.; Raston, C. L. *Chemistry of Organo-Zirconium and -Hafnium Compounds*; Wiley: New York, 1986; p 223.
(68) Tilley, T. D. *J. Am. Chem. Soc.* **1985**, *107*, 4084.
(69) Jeske, G.; Lauke, H.; Mauermann, H.; Swepston, P. M.; Schumann, H.; Marks, T. J. *J. Am. Chem. Soc.* **1985**, *107*, 8091.
(70) Kaminsky, W.; Külper, K.; Niedoba, S. *Macromol. Chem., Macromol. Symp.* **1986**, *3*, 377.
(71) Kaminsky, W.; Steiger, R. *Polyhedron* **1988**, *7*, 2375.
(72) Chien, J. C. W.; Wang, B.-P. *J. Polym. Sci., Part A: Polym. Chem.* **1990**, *28*, 15.
(73) Cowie, J. M. G. *Polymers: Chemistry and Physics of Modern Materials*; Chapman and Hall: New York, 1994; p 345.

Table 10. Ethylene Polymerization Activities and Polymer Properties[a]

precatalyst	cocatalyst	wt PE, g	time, min	activity (× 10^{-3}), g PE mol [M]$^{-1}$ h^{-1} atm^{-1}	10^{-3} M_n[b]	10^{-3} M_w[b]	10^{-3} M_z[b]	M_w/M_n[b]	mp,[c] °C
(Cp)(Trop)$ZrCl_2$ (**3**)	MMAO	1.916	2.5	9860	5.4	15	28	2.7	130
(Cp)(Trop)$Zr(CH_3)_2$ (**6**)[d]	$B(C_6F_5)_3$	0.17	0.51	3750	43	17	360	3.9	133
(Cp)(Trop)$TiCl_2$ (**4**)	MMAO	0.0063	7.2	10	23	78	59	3.3	124
$(Trop)_2ZrCl_2$ (**2**)[e]	MMAO	0.014	20.15	8	14	63	2100	44	129
Cp_2ZrCl_2	MMAO	0.383	0.55	8030	68	170	300	2.6	134
CpCp*$ZrCl_2$	MMAO	0.9885	1.5	7540					135
$CpZrCl_3$ [f]	MMAO	0.0053	32.1	2					123
$ZrCl_4$[e,f] (128)	MMAO	0.005	60.5	1					133
Cp_2TiCl_2 *f*	MMAO	0.583	2.25	2990					134
$CpTiCl_3$[f] (128)	MMAO	0.007	60.7	1					132

[a] Polymerization conditions: 100 mL toluene, 25 °C, 5.1 × 10^{-6} mol catalyst, 1000 Al/M, 1 atm ethylene. [b] By GPC. [c] By DSC; the numbers in parentheses indicate a minor peak in the DCS curve. [d] A 1:1 ratio of cocatalyst to precatalyst was used where 5.1 × 10^{-6} mol of precatalyst was used. [e] MMAO solution added to ethylene-saturated solution of toluene and the precatalyst. [f] Low detector response prohibited accurate GPC analysis.

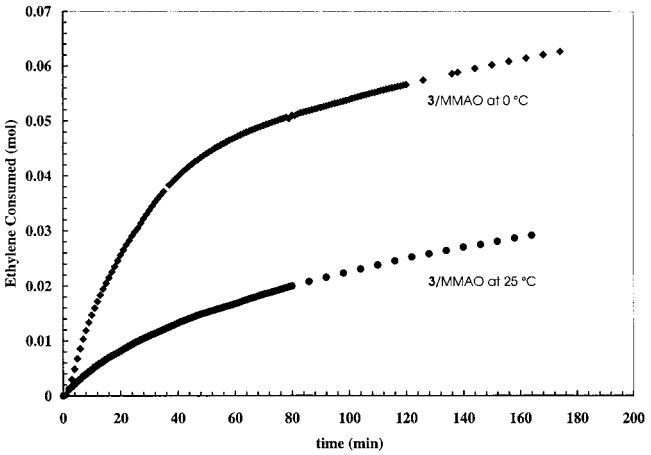

Figure 8. Ethylene uptake versus time during ethylene polymerization using (Cp)(Trop)$ZrCl_2$/MMAO at 25 °C (●) and 0 °C (◆).

3/MMAO system (Figure 8). Similar profiles were obtained using Cp_2ZrCl_2/MMAO. A higher activity was observed at 0 °C than at 25 °C.

α-Olefin Polymerization. Polymerization of propylene was carried out using (Cp)(Trop)MCl_2/MMAO catalyst systems in liquid propylene. The chain length of the resulting polymeric material was found to be metal dependent. High molecular weight polypropylene (PP) was generated using the **4**/MMAO system, and PP oligomer was generated using **3**/MMAO. The **2**/MMAO catalyst system failed to give any polymer or oligomer under the conditions employed in this study.

The catalyst **4**/MMAO in liquid propylene at 0 °C gave 0.62 g (activity = 37 g PP (mmol cat)$^{-1}$ h^{-1}) of rubbery PP. Analysis by GPC showed a bimodal distribution with the larger fraction being high molecular weight PP and a smaller fraction being lower molecular weight material in a ratio of 70:30. Analysis[74] of the molecular weight distribution of the larger fraction gave $M_w = 4.6 \times 10^5$, $M_n = 2.9 \times 10^5$, and $M_w/M_n = 1.6$; for the smaller fraction, $M_w = 1.6 \times 10^3$, $M_n = 2.09 \times 10^3$, and $M_w/M_n = 1.4$; overall the polydispersity was 49. The PP mixture was analyzed by $^{13}C\{^1H\}$ NMR spectroscopy, and the methyl region was resolved at the pentad level; the results are given in Table 11.[75] As can be seen by comparison of the experimental and calculated band intensities, the PP was mildly enriched in the syndiotactic pentads (rrrr and rrrm) and depleted in the isotactic pentads (mmmm and mmmr). Similar results were obtained at higher polymerization temperatures (25 °C). The $CpTiCl_3$/MMAO catalyst system failed to give any PP under these experimental conditions.

Table 11. Relative $^{13}C\{^1H\}$ NMR Methyl Pentad Intensity for PP Generated Using 4/MMAO[a]

pentad	experimental band intensity	theoretical band intensity for actactic PP
mmmm	0.03	0.06
mmmr	0.069	0.12
rmmr	0.058	0.06
mmrr	0.099	0.12
mmrm + rmrr	0.26	0.25
mrmr	0.129	0.12
rrrr	0.115	0.06
rrrm	0.17	0.12
mrrm	0.07	0.06

[a] See text for polymerization conditions.

The **3**/MMAO catalyst system in liquid propylene at 0 °C gave 1.4 g (activity = 59 g (mmol cat)$^{-1}$ h^{-1}) of an oily viscous liquid oligomer. Analysis by GC/MS showed a size range of C12 to C27.[76] End group analysis by ^1H NMR indicated that all unsaturated end groups contained the vinylidene ($CH_2C(CH_3)CH_2(R)$) functionality. On the basis of previous assignments, the $^{13}C\{^1H\}$ NMR spectrum was used to identify *n*-propyl, isobutyl, and vinylidene end groups in a 30:40:30 ratio and was consistent with a product generated from exclusive head-to-tail propylene insertion.[77,78]

Investigation of Active Catalyst Species. To gain further insight into the stability and properties of the active species involved in the polymerizations (and establish that the Trop ligands remain attached to the metal center), we carried out spectroscopic studies of the activation of precatalysts **3** and **6** using MMAO and $B(C_6F_5)_3$, respectively. A toluene solution of **3** was treated with 1000 equiv of MMAO, and the resulting mixture was quenched using excess $(n\text{-Bu})_3NHCl$ in toluene after ca. 2 min. Upon addition of MMAO before quenching, **3** was observed to be completely consumed

(74) Reference 73, pp 8−10.
(75) Ewen, J. *J. Am. Chem. Soc.* **1984**, *106*, 6355.
(76) The distribution of different molecular weight components was too narrow to be fit to a Schultz−Flory (most probable) distribution, possibly due to the isolated material not being representative of the actual oligomer distribution during polymerization. The oligomer distribution was found by GC to be (% composition, # of C atoms): (11, C12); (16, C15); (18, C18); (20, C21); (20, C24); (15, C27).
(77) Resconi, L.; Piemontesi, F.; Franciscono, G.; Abis, L.; Fiorani, T. *J. Am. Chem. Soc.* **1992**, *114*, 1025.
(78) Tsutsui, T.; Mizuno, A.; Kashiwa, N. *Polymer* **1989**, *30*, 428.

by UV−vis spectroscopy. After quenching with excess $(n\text{-Bu})_3$NHCl, the dichloride **3** was regenerated quantitatively within the uncertainty limits of this experiment (ca 15%). Upon addition of 5 equiv of MMAO to a toluene-d_8 solution of **3**, a color change from orange to light red was observed. After quenching the reaction mixture with excess $(n\text{-Bu})_3$NHCl the original orange color was restored and **3** was generated in 88% yield by ^{1}H NMR spectroscopy in the presence of an inert internal standard (ferrocene).

In the triarylborane experiments, we employed the activation methodology developed by Marks and coworkers.[79,80] Treating complex **6** with 1 equiv of the methide-abstracting agent $B(C_6F_5)_3$ in toluene-d_8 or chlorobenzene-d_5 resulted in the immediate formation of a red solution formulated as the methyltriarylborate complex $[(Cp)(Trop)ZrCH_3][CH_3B(C_6F_5)_3]$ (**14**) (eq 8). The ^{1}H NMR spectrum exhibited a single Cp resonance,

$$\underset{\mathbf{6}}{(Cp)(Trop)ZrMe_2} + B(C_6F_5)_3 \longrightarrow \underset{\mathbf{14}}{[(Cp)(Trop)ZrMe][MeB(C_6F_5)_3]} \quad (8)$$

three resonances in the allyl and bridgehead region in a 1:2:2 ratio, two resonances corresponding to methylene protons, and methyl resonances corresponding to NMe, BMe, and ZrMe in a 1:1:1 ratio. The ^{11}B NMR spectrum exhibited a single resonance at −15 ppm, consistent with the presence of a tetrahedral borate anion.[81] The ^{19}F NMR spectrum showed a single three-resonance pattern and indicated that all of the starting borane was consumed. A large chemical shift difference (5 ppm) between the meta and para fluorine resonances of the borate was observed, indicative of coordination of the borate anion to a cationic zirconium metal center.[23,82] The complex was only moderately stable in toluene-d_8 at room temperature ($t_{1/2} = 1$ h) and less stable in more polar solvents. Approximate room-temperature half-lives ($t_{1/2}$) for decomposition in chlorobenzene-d_5 and CD_2Cl_2 were 0.5 and 0.1 h, respectively; however, solutions of **14** in chlorobenzene-d_5 at < 0 °C were stable for many hours. Upon cooling a solution of **14** to −20 °C, the resonances corresponding to the allyl and bridgehead protons began to broaden. The line shape of two separate resonances for the ZrMe and the BMe groups remained unchanged relative to other nonexchanging resonances upon lowering the temperature. The line shape of the central allyl resonance also remained unchanged, but the chemical shift was found to move slightly upfield. These changes were similar to the spectral changes observed upon cooling a CD_2Cl_2 solution of $(Cp)(Trop)TiMe_2$ (**7**) (see Figure 6). The ^{1}H NMR spectrum of complex **14** could not be obtained in the slow-exchange regime due to the limited liquid range of the solvent; this precluded estimation of the energetic barrier for this exchange process.

Discussion

Synthesis and Structure of Tropidinyl Metal Complexes. Traditional synthetic routes for coordination of Cp ligands to group 4 metal centers have relied heavily on the use of thallium, magnesium, and alkali metal cyclopentadienide reagents.[67] The use of tri(alkyl)-tin-mediated transmetalation of Cp rings has not been used as extensively by comparison. The tin reagent $CpSnR_3$ has only received modest attention for early metal systems because other methods are highly effective.[83−86] The silicon reagent $CpSiMe_3$ has been similarly employed to coordinate Cp ligands to Ti metal centers where electrophilic attack of the Cp group with cleavage of the Si−C bond was thought to occur.[87] Use of the traditional methods was not successful in the Trop series, but the tin reagent **1** proved to be a convenient and stable source of the Trop ligand[88] and was shown to readily undergo transmetalation with group 4 chlorides. When coordinatively more saturated forms of the group 4 metal halides such as $ZrCl_4\cdot(THF)_2$ or $CpZrCl_3\cdot$DME were used, undesired byproducts were produced. This observation suggests that initial coordination of the nitrogen atom in **1** to the unsaturated group 4 metal chloride may facilitate transmetalation to form the η^3-allyl functionality.

Syntheses of metallocene dialkyl complexes from the parent dichlorides proceed readily by treating group 4 metallocene dihalides with lithium or magnesium alkyl reagents.[89] In contrast to the Trop-attachment reactions, similar routes were effective for the alkylation of complexes bearing the Trop ligand. The dialkyl complexes also displayed reactivity similar to that of the corresponding dialkylmetallocenes.[90]

Determination of several X-ray structures shows the Trop ligand can be either symmetrically or unsymmetrically orientated with respect to the metal wedge. The symmetric mode, observed in **2**, **3**, and **5,** can be described as having the NMe group bisecting the wedge of the Zr coordination sphere.[91] An unsymmetric orientation of the Trop ligand was observed in complexes **2**, **5**, **8**, and **13**, where the NMe group is directed away from one of the ligands in the wedge.

Fluxional Behavior of Complexes Bearing the Trop Ligand. The solid-state structures of the complexes bearing the Trop ligand, with the exception of **3**, were less symmetric than would be predicted on the basis of their NMR spectra obtained at room temperature. Variable-temperature NMR studies revealed dynamic processes occurring in solution. Two exchange processes accounted for the increased complexity of the

(79) Yang, X.; Stern, C. L.; Marks, T. J. *J. Am. Chem. Soc.* **1991**, *113*, 3623.
(80) Yang, X.; Stern, C. L.; Marks, T. J. *J. Am. Chem. Soc.* **1994**, *116*, 10015.
(81) Kidd, R. G. *Boron-11*; Academic Press: New York, 1983; Vol. 2, pp 49−50.
(82) Horton, A. D.; de With, J. *Chem. Commun.* **1996**, 1375.
(83) Lund, E. C.; Livinghouse, T. *Organometallics* **1990**, *9*, 2426.
(84) Spetseris, N.; Hadida, S.; Curran, D. P.; Meyer, T. Y. *Organometallics* **1998**, *17*, 1458.
(85) Nifant'ev, I. E.; Ivchenko, P. V. *Organometallics* **1997**, *16*, 713.
(86) Lisowsky, R. Eur. Pat. Appl. 669340 A 1, 1995.
(87) Cardoso, A. M.; Clarke, R. J. H.; Moorhouse, S. *J. Chem. Soc., Dalton Trans.* **1980**, 1156.
(88) The lithiated anion (TropLi) was found to be unstable at temperatures above −78 °C, and preparations using this species were cumbersome. See ref 45 for the details of using Li salts directly for the synthesis of metal complexes.
(89) Jeffery, J.; Lappert, M. F.; Luong-Thi, M. F.; Webb, N. T. A., J. L.; Hunter, W. E. *J. Chem. Soc., Dalton Trans.* **1981**, 1593.
(90) Lappert, M. F., Abel, E. W., Stone, F. G. A., Wilkinson, G., Eds. *Comprehensive Organometallic Chemistry*; Pergamon Press: Oxford, 1982; Vol. 3, p 580.
(91) Neither of the NMe groups bisects the C17−Zr−C24 angle of complex **8** and would not be considered to be in a symmetric orientation as described in the text; however, one Trop ligand adopts an unsymmetric orientation. It is possible that the distortion of the Trop ligand from the symmetric orientation is brought about by steric repulsion between the NMe and the large benzyl groups.

NMR spectra upon lowering the temperature. One process involves interconversion of enantiomers (complexes **2** and **7**). The other involves interconversion of diastereomers (complexes **3** and **4**). The fluxionality of group 4 metallocene complexes has been found to be important in determining the selectivity of olefin insertions into a growing polymer chain.[92−95] The implications for improving the selectivity of olefin insertion based on the fluxional properties of the Trop ligand prompted us to study the dynamic behavior of these complexes.

Complex **7** exists as a single diastereomer that undergoes interconversion of enantiomers, giving rise to an averaged C_s symmetric structure by ^{1}H NMR spectroscopy at ambient temperature. Similar enantiomer exchange processes have been observed with other metallocene[96] and π-allyl[97] complexes. A fluxional process that accounts for the spectral changes observed in Figure 6 is shown in eq 9. The Trop ligand binds to the

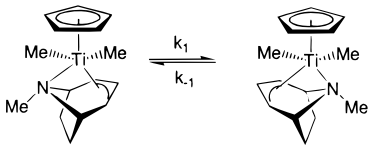

(9)

metal in an unsymmetric fashion, giving rise to two TiMe resonances and five allyl and bridgehead resonances in the low-temperature (−90 °C) ^{1}H NMR spectrum.

The solid-state structure of **2** shows that the Trop ligands are inequivalent (Figure 1). The ^{1}H NMR spectrum of complex **2** exhibited time-averaged C_{2v} symmetry and was consistent with rapid rotation of the Trop ligands.[96] A fluxional process similar to that postulated for **7**, which results in interconversion of enantiomers, is illustrated in eq 10 and accounts for the temperature dependence of the ^{1}H NMR spectrum (Figure 4).

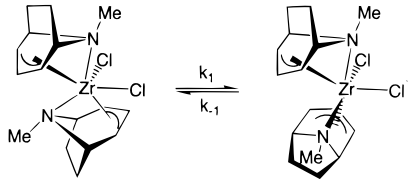

(10)

The dichloride complex (Cp)(Trop)$TiCl_2$ (**4**) at room temperature in CD_2Cl_2 solution was found to exist as a mixture of two diasteromers in unequal populations. At room temperature the symmetric isomer is more heavily populated than the unsymmetric isomer. Once again rotation of the Trop ligand relative to the metal wedge accounts for these observations (eq 11). Complex **3**

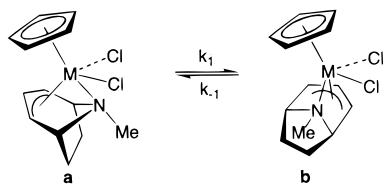

a **b**

M = Zr (**3**), Ti (**4**)

(11)

exhibited similar behavior, with the exception that a much lower barrier was found for the interconversion of its isomers and the population differences between **3a** and **3b** were more pronounced. We suggest that the large difference in the interconversion free energy barriers of complexes **3** and **4** is predominantly steric and results from the size difference between zirconium and titanium. The smaller titanium atomic radius forces the Trop ligand to lie closer to the metal center relative to zirconium, resulting in a higher isomerization barrier.

Polymerization Catalysis. Several qualitative comparisons can be made from the data in Table 10. The activity of **3**/MMAO is similar to that of Cp_2ZrCl_2/MMAO. The less hindered mixed Cp/Trop complex **3**/MMAO is more active than the more hindered (bis)-Trop complex **2**/MMAO. The broad polydispersity and bimodal nature (by GPC) of the PE generated from the **2**/MMAO catalyst suggests that more than one active species may be generated in this system. The titanium complex **4**/MMAO also displayed a lower activity than **3**/MMAO and generated more highly branched PE, as evidenced by the lower melting temperature. The **6**/$B(C_6F_5)_3$ catalyst system exhibited activity comparable to that of the **3**/MMAO system, but the resulting PE had a much higher molecular weight and broader polydispersity. The M_w of the polymer generated from **3**/MMAO was much lower than that observed for Cp_2ZrCl_2/MMAO, indicating that chain transfer was more facile for the Trop-bearing complex. The activities of **2**/MMAO, **3**/MMAO, and **4**/MMAO were all higher than the activities of the parent metal chlorides $ZrCl_4$, $CpZrCl_3$, and $CpTiCl_3$ run under identical conditions. These observations indicate that at least to some degree the Trop ligand enhances the reactivity of the metal centers under our polymerization conditions relative to the metal chloride precursors.

The ethylene uptake experiments indicate that for **3**/MMAO an active catalyst system was present in solution over the course of hours. The results obtained in this study were similar to the ethylene uptake profile observed for Cr catalyst systems.[98,99] Analogous uptake profiles were observed for Cp_2ZrCl_2/MMAO under identical conditions.

Both the zirconium and titanium (Cp)(Trop)MCl_2/MMAO catalyst systems polymerized propylene. The titanium system produced much higher molecular weight PP than the zirconium system. This is likely due to differing chain transfer rates for these two systems. The more sterically encumbered Ti system exhibits an apparently higher barrier for chain transfer.[77] Similarly, Ewen has observed that higher molecular weight PP was generated from $CpCp^*ZrCl_2$/MAO in comparison to the less sterically bulky Cp_2ZrCl_2/MAO system. Kaminski et al. have also demonstrated that methyl substitu-

(92) Maciejewski-Petoff, J. L.; Bruce, M. D.; Waymouth, R. M.; Masood, A. M.; Lal, T. K.; Quan, R. W.; Behred, S. J. *Organometallics* **1997**, *16*, 5909.

(93) Bruce, M. D.; Coates, G. W.; Hauptman, E.; Waymouth, R. M.; Ziller, J. W. *J. Am. Chem. Soc.* **1997**, *119*, 11174.

(94) Knickmeier, M.; Erker, G.; Fox, T. *J. Am. Chem. Soc.* **1996**, *118*, 9623.

(95) Erker, G.; Aulbach, M.; Knickmeier, M.; Wingbermühle, D.; Krüger, C.; Nolte, M.; Werner, S. *J. Am. Chem. Soc.* **1993**, *115*, 4590.

(96) Luke, W. D.; Streitwiser, A., Jr. *J. Am. Chem. Soc.* **1981**, *103*, 3241.

(97) Buchmann, B.; Piantini, U.; von Philipsborn, W.; Salzer, A. *Helv. Chim. Acta* **1987**, *70*, 1487.

(98) Thomas, B. J.; Noh, S. K.; Schulte, G. K.; Sendlinger, S. C.; Theopold, K. H. *J. Am. Chem. Soc.* **1991**, *113*, 893.

(99) Bhandari, G.; Kim, Y.; McFarland, J. M.; Rhingold, A. L.; Theopold, K. H. *Organometallics* **1995**, *14*, 738.

Scheme 4

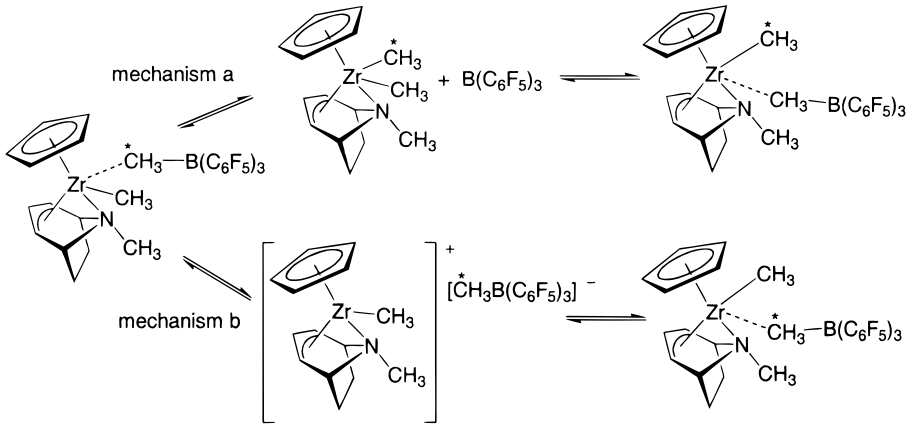

tion on cyclopentadienyl rings slows down the chain transfer step relative to the ethylene insertion. This resulted in higher molecular weight PE for the CpCp*$ZrCl_2$/MAO and Cp*$_2ZrCl_2$/MAO systems relative to that for Cp_2ZrCl_2/MAO.[70]

Resconi et al.[77] have analyzed the end groups of propylene oligomers by $^{13}C\{^1H\}$ NMR. They noted that the presence of *n*-propyl and isobutyl end groups are indicative of a β-H elimination mechanism[100] for chain transfer, and the presence of isobutyl end groups is consistent with an aluminum chain transfer mechanism.[101] For the **3**/MMAO catalyst system, based on the end groups present in the isolated oligomer, the predominant chain transfer mechanism involves β-H elimination. For this catalyst system no evidence was found for a β-Me elimination chain transfer pathway.[102]

Nature of the Active Catalyst Species. Mack and Eisen have shown that amide ligands can be abstracted by strong Lewis acids such as MAO.[103] Attack upon the Trop ligand by a strong Lewis acid like MMAO could convert the complex to a non-Trop-bearing catalyst during the polymerization or deactivate the catalyst system. Experiments were carried out to determine whether the Trop ligand remained intact for precatalyst **3** upon treatment with MMAO. As described above, **3** is regenerated in good yield after activation using MMAO by adding excess $(n\text{-Bu})_3NHCl$ as a quenching reagent. These results suggest that that for complex **3** the Trop ligand remains at least substantially intact during the time of the polymerizations used in this study.[104]

From the data in Table 10, it can be seen that the complexes bearing the Trop ligand exhibited higher activities than their corresponding parent metal halides. These observations reinforce our judgment that the Trop ligand remains coordinated during the polymerization catalysis. However, the increase in catalytic activity, for the generation of PE using complexes **2** and **4**, imparted by coordination of the Trop ligand was modest at best. Furthermore, the **4**/MMAO catalyst system generated PP, while the $CpTiCl_3$/MMAO system failed to generate any PP, indicating that the Trop ligand also imparts enhanced catalytic reactivity to this complex for the polymerization of propylene.

To further our understanding of the active catalyst species, we generated catalyst system **6**/$B(C_6F_5)_3$ and found it to be highly active for the polymerization of ethylene (Table 10). Spectroscopic investigation revealed the presence of the cationic zirconium complex [(Cp)(Trop)ZrMe][$MeB(C_6F_5)_3$] (**14**).[79,80] Both sides of the Trop ligand in **14** were equivalent at 20 °C in a C_6D_5Cl solution, indicating that an exchange process permutes both sides of the diastereotopic Trop ligand.

Two general mechanisms have been proposed for exchange of diastereotopic groups on the ancillary ligands in group 4 metallocinium ions generated by methide abstraction using $B(C_6F_5)_3$.[80,105,106] These mechanisms as applied to complex **14** are shown in Scheme 4. One exchange pathway involves dissociation of $B(C_6F_5)_3$ to form two neutral species, followed by reabstraction of the unique ZrMe group; this is denoted as the borane dissociation mechanism (mechanism a). The other mechanism involves ion-pair separation to form a solvent-separated cation/anion pair followed by reassociation; this is denoted as the ion pair dissociation−recombination mechanism (mechanism b). The former mechanism exchanges *both* the ZrMe/BMe groups *and* the diastereotopic groups on the ligand, while the latter mechanism *only* exchanges diastereotopic groups on the ligands. At low temperature in C_6D_5Cl the borane disassociation mechanism (a) is apparently much slower than the ion-pair separation mechanism (b) since the ZrMe and BMe resonances were clearly separated and no broadening was observed relative to the line shapes of nonexchanging resonances. Similar results were observed for [(1,2-$(CH_3)_2C_5H_3)_2$ZrMe][$CH_3B(C_6F_5)_3$], where the rate for ion-pair dissociation was observed to be 10^3 times faster than the rate of borane dissociation at 25 °C in C_6D_5Cl.[106] The instability of **14** precluded heating the sample to measure the barrier for borane dissociation. Qualitatively, we can say from the current set of experiments that as observed in Marks' system, ion-pair dissociation (mechanism b) is more facile than that of borane dissociation (mechanism a) at the temperatures employed in this study.

(100) Kaminsky, W.; Ahlers, A.; Möller-Lindenhof, N. *Angew. Chem., Int. Ed. Engl.* **1989**, *28*, 1216.
(101) Resconi, L.; Bossi, S.; Abis, L. *Macromolecules* **1990**, *23*, 4489.
(102) Eshuis, J. J. W.; Tan, Y. Y.; Teuben, J. H.; Renkema, J. *J. Mol. Catal.* **1990**, *62*, 277.
(103) Mack, H.; Eisen, M. S. *J. Organomet. Chem.* **1996**, *525*, 81.
(104) It is of course difficult to rule out the possibility that only a small concentration of an extremely active "unknown" catalyst is responsible for the majority of the polymer produced.
(105) Deck, P. A.; Marks, T. J. *J. Am. Chem. Soc.* **1995**, *117*, 6128.
(106) Deck, P. A.; Beswick, C. L.; Marks, T. J. *J. Am. Chem. Soc.* **1998**, *120*, 1772.

Conclusion

Using a stannyltropidine reagent, a new class of group 4 complexes bearing the tropidinyl ligand have been synthesized and their properties investigated. The metal complexes display fluxional behavior, and the exchange pathways responsible for these observations were investigated. The dialkyl complexes display reactivity akin to that of the analogous Cp complexes. Some of the complexes were shown to be active polymerization catalysts when combined with an appropriate cocatalyst. Upon activation with MMAO, the (Cp)(Trop)$ZrCl_2$ (**3**) precatalyst system displayed PE activities and lifetimes similar to those of Cp_2ZrCl_2/MMAO. Two Trop-based catalyst systems (**3**/MMAO and **4**/MMAO) were shown to polymerize propylene. The nature of the active catalyst species was investigated by methide abstraction from (Cp)(Trop)$ZrMe_2$ (**6**) using tris(pentafluorophenyl)-borane. The observed cationic complex was less stable than, but displayed similar dynamic behavior to, metallocene systems. Current efforts are directed toward developing synthetic routes to *ansa*-Trop complexes and adding substituents to the Trop ligand to investigate and improve the selectivity and/or activity of the catalyst systems.

Experimental Section

General Methods. All reactions were performed under an inert atmosphere (Ar or N_2) using standard glovebox or Schlenk techniques.[107] All infrared (IR) spectra were recorded on a Mattson Galaxy series FT-IR 3000 spectrometer. UV−vis experiments were preformed using a Hewlett-Packard 8453 UV−vis spectrometer. Gas chromatography was carried out using a Hewlett-Packard 5890 series II instrument using a 60 m J and W Scientific DB-XLB column equipped with a flame ionization detector. GC/MS analysis was carried out using a Hewlett-Packard 6890 series GC system, equipped with a 30 m DB-XLB column, with a Hewlett-Packard model 5973 mass selector detector using an ionization voltage of 70 eV. Mass spectrometric (MS) analyses were performed at the University of California, Berkeley Mass Spectrometry facility on a AEI MS-12 and Kratos MS-50 mass spectrometers. Elemental analyses were performed by the University of California, Berkeley Microanalytical facility. X-ray structural analyses were performed at the University of California, Berkeley CHEXRAY facility. DSC analysis was performed on a TA Instruments DSC 2010 differential scanning calorimeter at a heating rate of one deg min^{-1}. GPC analyses of the PE and PP samples were carried out using a Waters 150 C+ instrument at 145 °C in 1,2,4-trichlorobenzene and calibrated using a standard sample of PE or PP.

Unless otherwise noted, all reagents were purchased from Aldrich and used without further purification, and **1** was synthesized as described previously.[45] The metal halides $CpZrCl_3$ and $CpTiCl_3$ were purchased from Strem Chemicals, and 2,6-dimethylisocyanate was purchased from Fluka and dried over 4 Å sieves as an ethereal solution. MMAO was purchased from Akzo-Nobel, and tris(pentafluorophenyl)borane was obtained from Albemarle. Polymer grade ethylene and propylene were purified by passage though a Matheson model 6427-46 oxygen/moisture trap. Potassium bromide (Aldrich), Celite (Aldrich), silica gel (Merck 60, 230−400), and alumina (Brockman I, Aldrich) were dried in vacuo at 250 °C for 48 h. Toluene, pentane, hexanes, methylene chloride, and benzene (Fisher) were passed through a column of activated alumina (type A2, size 12 × 32, Purifry Co.) under nitrogen pressure and sparged with N_2 prior to use. Diethyl ether and tetrahydrofuran (Fisher) were distilled from purple sodium/benzophenone ketyl under N_2 prior to use. All deuterated solvents were purchased from Cambridge Isotope Laboratories. Benzene-d_6, toluene-d_8, and THF-d_8 were vacuum transferred from purple sodium/benzophenone ketyl solutions, and CD_2Cl_2 was vacuum transferred from CaH_2. Chlorobenzene-d_5 and $C_2D_2Cl_4$ were degassed, stored over 4 Å sieves, and filtered through dry Celite before use.

NMR Spectroscopy. NMR experiments were performed on a Bruker AMX spectrometer resonating at 300.13 MHz for ^1H that was equipped with an inverse probe. One-dimensional $^{13}C\{^1H\}$ spectra and DEPT spectra were recorded on either a Bruker AMX spectrometer resonating at 400 MHz for ^1H or 100 MHz for ^{13}C that was equipped with a QNP probe or a Bruker DRX spectrometer resonating at 500 MHz for ^1H or 125 MHz for ^{13}C that was equipped with a broad band probe. The 2D EXSY spectrum was acquired in phase-sensitive mode using the Bruker pulse program noesytp at 298 K. NMR analyses of the PP samples were carried out in $C_2D_2Cl_4$ at 100 °C using 1% polymer loading for the long-chain PP and 10% polymer loading for PP oligomer.

Ethylene Polymerization Experiments. The following adapted procedure was used for the ethylene polymerization experiments.[69] Reactions were carried out in oven-dried 250 mL Schlenk flasks with a straight bore stopcock capped with a septum equipped with a large stir bar and a Teflon valve attached to a ground glass joint. The flask was charged with 100 mL of toluene inside a glovebox and then attached to a vacuum line. The toluene was degassed, allowed to saturate under 1 atm of ethylene, and then brought to the reaction temperature using a Neslab Endocal LT-50DD constant temperature controller. The catalyst solutions were prepared in the glovebox by adding a known quantity of MMAO (2.2 mL of a 2.3 M solution) to a weighed sample of the group 4 precatalyst. The catalyst solution was loaded into a syringe, removed from the glovebox, and quickly added to the reaction flask through the septum-capped straight bore stopcock. The polymerization reaction was allowed to proceed with constant stirring and stopped by venting the monomer and immediately quenching with 3 mL of 10% aqueous concentrated HCl/methanol. The resulting polyethylene was filtered, washed with 10% HCl, water, and methanol, and dried in an oven or under vacuum to a constant weight. By performing multiple runs using the same catalysts the precision of the activities measured using this method was found to fall within a factor of 2 of each other. Ethylene uptake measurements were performed using a MKS Baratron pressure gauge to monitor the pressure drop using a setup described in the literature.[98]

Propylene Polymerization Experiments. All propylene polymerizations were carried out in neat propylene in a 3 oz Lab Crest glass (rated to 200 psig) reactor with a stir bar using a modification of an established procedure.[108] The flask was charged with 0.322 g of solid MMAO (dried by removing the toluene under reduced pressure and exposing to high vacuum for 48 h) in the glovebox. The flask was then sealed and the entire reactor assembly removed from the glovebox. The reactor was equipped with an inlet valve, stir bar, pressure gauge, a septum port (stainless steel ball valve with a silicone rubber septum) placed in a 1/4 in. compression fitting, and a pressure relief valve set to 175 psig. The reactor was then attached to the propylene line, and the inlet valve was purged with propylene for 2 min at 25 psig. The flask was cooled to −78 °C, and propylene (∼50 mL) was then condensed into the cooled reaction flask. The reactor assembly was protected with

(107) Burger, B. J.; Bercaw, J. E. *Vacuum Line Techniques for Handling Air-Sensitive Organometallic Compounds*; In Wayda, A. L., Darensbourg, M. Y., Eds. *Experimental Organometallic Chemistry*; American Chemical Society: Washington D.C., 1987; Vol. 357, pp 79−98.

(108) Herzog, T. A.; Zubris, D. L.; Bercaw, J. E. *J. Am. Chem. Soc.* **1996**, *118*, 11988.

a safety shield and allowed to warm to 0 °C. The catalyst solutions were prepared in the glovebox (~2 mg or 0.0051 mmol precatalyst in 0.5 mL of either dichloromethane or toluene) and loaded into a 1 mL Hamilton gastight syringe with a ground glass luer tip and a 5 in. 15 gauge stainless steel needle attached with ITW Devon 5 Minute epoxy. The precatalyst solution was removed from the glovebox and then injected through the septum port to initiate the reaction. The polymerizations were allowed to proceed with constant stirring for 4 h, after which time the monomer was slowly vented and the reaction quenched with 3 mL of 10% aqueous concentrated HCl/methanol. The high molecular weight polypropylene was scraped from the walls of the reaction flask and washed with water and methanol, dried under vacuum, and weighed. After quenching the reaction liquid oligomer was extracted using pentane, separated from the aqueous layer, dried over $MgSO_4$, filtered, then concentrated using rotary evaporation.

(Trop)$_2$ZrCl$_2$ (2). A Schlenk flask was charged with a solution of $ZrCl_4$ (0.391 g, 1.68 mmol) in CH_2Cl_2 (12 mL). The tin reagent **1** (0.959 g, 3.35 mmol) was slowly added. The solution immediately turned orange and was stirred for 4 h at room temperature. The reaction mixture was filtered and the solid extracted with CH_2Cl_2 (2 × 3 mL). The volatile materials were removed from the filtrate under reduced pressure, and the residue was washed thoroughly with pentane and then extracted with toluene. The solvent was removed under vacuum to give 0.572 mg (46%) of an analytically pure fine orange powder. ^{1}H NMR (300 MHz, CD_2Cl_2, 20 °C and −90 °C): see Table 6. ^{1}H NMR (300 MHz, C_6D_6, 20 °C): δ 5.38 (t, J = 7.3 Hz, 2H, central allylic), 4.26 (br s, 4H, terminal allylic), 3.54 (br s, 4H, bridgehead), 2.29 (s, 6H, N*Me*), 1.84 (s, 4H, CH_2), 1.68 (m, 4H, CH_2). ^{13}C{^{1}H} NMR (100 MHz, CD_2Cl_2, 20 °C): δ 132.0 (central allylic) 87.6 (terminal allylic), 67.0 (bridgehead), 41.2 (N*Me*), 38.9 (*C*H$_2$). Anal. Calcd for $C_{16}H_{24}N_2Cl_2Zr$: C, 47.28; H, 5.95; N, 6.89. Found: C, 46.78; H, 5.85; N, 6.60. HRMS calcd: 404.0364. Found: 404.0361.

(Cp)(Trop)ZrCl$_2$ (3). A solution of **1** (3.03 g, 7.86 mmol) was added to a suspension of $CpZrCl_3$ (2.03 g, 7.73 mmol) in CH_2Cl_2 (100 mL). Upon addition of the tin reagent the solution immediately turned orange. The solution became homogeneous, and it was allowed to stir for 45 min. The solvent was removed under reduced pressure. The crude product was washed with pentane (3 × 60 mL), and the material was placed under vacuum for 12 h. The crude material was taken up in a minimum amount of CH_2Cl_2 (100 mL) and filtered through glass fiber filter paper into a 250 mL round-bottom Schlenk flask. Then 100 mL of pentane was slowly added, and an orange precipitate immediately formed. The flask was attached to a swivel frit assembly, cooled to −78 °C, and allowed to stir for 0.5 h. The orange precipitate was collected by filtration at −78 °C. The material was then washed with pentane and dried under vacuum (2.19 g, 81% yield). Analytically pure material was obtained by slow cooling (−40 °C) of a saturated CH_2Cl_2 solution to afford crystals of **3**. ^{1}H NMR (300 MHz, CD_2Cl_2, 20 °C and −70 °C): see Table 6. ^{1}H NMR (300 MHz, C_6D_6, RT): δ 5.89 (5H, s, C_5H_5), 4.76 (1 H, br, central allylic), 3.82 (2H, br, terminal allylic), 3.56 (2H, br, bridgehead), 2.40 (3H, br, NCH_3), 1.69−1.59 (4H, m, CH_2). ^{13}C{^{1}H} (100 MHz, CD_2Cl_2, 20 °C): δ 129.9 (central allylic), 114.2 (C_5H_5), 88.0 (terminal allylic), 66.4 (bridgehead), 40.2 (N*C*H$_3$), 38.3 (*C*H$_2$). UV (toluene) λ_{max}, nm (ϵ): 421 (1,371). MS (EI): m/z 347 (M$^+$). Anal. Calcd for $C_{13}H_{17}Cl_2NZr$: C, 44.69; H, 4.90; N, 4.01. Found: C, 44.42; H, 4.98; N, 3.75.

(Cp)(Trop)TiCl$_2$ (4). A solution of **1** (0.625 g, 2.18 mmol) in CH_2Cl_2 (3 mL) was added to a suspension of $CpTiCl_3$ (0.471 g, 2.14 mmol) in CH_2Cl_2 (3 mL). The color of the solution immediately changed from orange to yellow to green, and the reaction was allowed to proceed for 12 h. The solvent was removed under reduced pressure, and the green residue was washed with pentane (3 × 5 mL) and left under dynamic vacuum for 12 h. Finally, the green solid was taken up in CH_2Cl_2 and filtered through glass fiber filter paper, the solvent removed under reduced pressure, and the mixture left under vacuum for 12 h to give 0.65 g (97%) of analytically pure **4**. Complex **4** was isolated as a mixture of two isomers (see text). ^{1}H NMR (300 MHz, $CDCl_3$, 100 °C and CD_2Cl_2 20 °C): see Table 6. ^{13}C{^{1}H} (125 MHz, CD_2Cl_2, RT): δ (isomer **4a**) 123.58 (central allylic), 118.32 (C_5H_5), 102.90 (terminal allylic), 66.72 (bridgehead), 40.46 (N*C*H$_3$), 35.24 (*C*H$_2$); (isomer **4b**) 132.21 (central allylic), 123.58 (terminal allylic), 119.56 (C_5H_5), 88.93 (terminal allylic), 67.62 (bridgehead), 64.43 (bridgehead), 42.78 (N*C*H$_3$), 35.46 (*C*H$_2$), 34.25 (*C*H$_2$). MS (EI): m/z 305 (M$^+$). Anal. Calcd for $C_{13}H_{17}Cl_2NTi$: C, 51.01; H, 5.60; N, 4.58. Found: C, 50.69; H, 5.70; N, 4.27.

(Trop)$_2$ZrMe$_2$ (5). The zirconium dichloride complex **2** (118 mg, 0.290 mmol) was dissolved in 10 mL of THF and cooled to −30 °C. Methyllithium (0.41 mL, 1.4 M in Et_2O) was added, and the reaction mixture was stirred at room temperature for an additional 3.5 h. The solvent was evaporated under reduced pressure, and the residue was extracted with pentane. The combined pentane extracts were filtered through Celite. The filtrate was recovered, and the volatile materials were removed under vacuum to yield 94.6 mg (89%) of analytically pure yellow solid. ^{1}H NMR (300 MHz, CD_2Cl_2, 20 °C): see Table 3. ^{1}H NMR (C_6D_6): δ 4.86 (dd, J = 7.4 Hz, 2H, central allylic), 3.87 (q, J = 7.3 Hz, 4H, terminal allylic), 3.31 (br, 4H, bridgehead), 2.12 (m, 4H, CH_2), 2.02 (s, 6H, N*Me*), 1.90 (m, 4H, CH_2), 0.22 (s, 6H, Zr*Me*$_2$). ^{13}C{^{1}H} (100 MHz, CD_2Cl_2, 20 °C): δ 149.7 (central allylic), 103.9 (terminal allylic), 90.1 (bridgehead), 63.9 (N*Me*), 63.2 (*C*H$_2$), 47.6 (Zr*Me*$_2$). ^{13}C{^{1}H} NMR (100 MHz, C_6D_6, 20 °C): δ 126.3 (central allylic), 80.4 (terminal allylic), 66.8 (bridgehead), 40.4 (N*Me*), 39.9 (*C*H$_2$), 25.8 (Zr*Me*$_2$). Anal. Calcd for $C_{18}H_{30}N_2Zr$: C, 59.12; H, 8.27; N, 7.66. Found: C, 59.43; H, 8.38; N 7.60. LRMS (EI), m/z: calcd 364. Found: 364.

(Cp)(Trop)ZrMe$_2$ (6). To a cooled (−30 °C) suspension of **3** (0.467 g, 1.34 mmol) in Et_2O (10 mL) was added methyllithium (1.86 mL, 1.45 M in ether) over a period of 5 min. The mixture was allowed to react for 1 h at −30 °C and finally warmed to room temperature. The supernatant was filtered through a pad of Celite, the filter cake was washed with Et_2O (3 × 2 mL), and the solvent was removed under reduced pressure. The crude product was extracted with pentane (3 × 5 mL), and the combined fractions were filtered through glass fiber filter paper. The solution was concentrated to 8 mL and cooled to −30 °C for 12 h, and yellow crystals were isolated to give 0.253 g of **6**. The resulting supernatant was then concentrated to 5 mL to give a second crop (0.043 g, 72% combined yield). The product was observed to decompose upon prolonged exposure to dynamic vacuum. ^{1}H NMR (300 MHz, CD_2Cl_2, 20 °C): see Table 6. ^{1}H NMR (300 MHz, C_6D_6, RT): δ 5.77 (5H, s, C_5H_5), 4.34 (1H, J = 7.5 Hz, central allylic), 3.84 (2H, q, J = 7.2, 4.5, terminal allylic), 3.18 (2H, br, bridgehead), 1.99 (2H, q, J = 10.2, 4.5, CH_2), 1.86 (3H, br, NCH_3), 1.78−1.72 (2 H, m, CH_2).). ^{13}C{^{1}H} (125.75 MHz, C_6D_6, RT): δ 123.1 (CH, central allylic), 109.6 (CH, C_5H_5), 79.9 (CH, terminal allylic), 66.3 (CH, bridgehead), 39.8 (CH_3, N*Me*), 39.5 (CH_2), 27.0 (CH_3, Zr*Me*). HRMS (EI) m/z M$^+$ calcd for $C_{15}H_{23}NZr$: 307.087. Found: 307.088 (a ^{1}H NMR spectrum of purified material used to obtain the HRMS is provided in the Supporting Information).

(Cp)(Trop)TiMe$_2$ (7). Methyllithium (0.6 mL, 1.4 M in Et_2O) was added to a cooled (−30 °C) suspension of (Cp)(Trop)-$TiCl_2$ (**4**) (0.128 g, 0.42 mmol) in Et_2O (4 mL). The reaction was allowed to proceed at −30 °C for 1.5 h. The red/brown supernatant was separated from the LiCl by filtration through a pad of Celite while still somewhat cold and the Et_2O removed under reduced pressure. The resulting red solid was extracted with pentane (3 × 3 mL), filtered through glass fiber filter paper, concentrated to 6 mL, and cooled to −30 °C for 12 h. Red needles were then harvested to give 0.065 g (58% yield) of analytically pure material. ^{1}H NMR (500 MHz, CD_2Cl_2, 20

°C and −80 °C): see Table 6. $^{13}C\{^1H\}$ (125.75 MHz, CD_2Cl_2, RT): δ 128.78 (CH, central allylic), 113.61 (CH, C_5H_5), 65.99 (CH, bridgehead), 41.25 (CH_3, N*Me*), 37.59 (CH_2). $^{13}C\{^1H\}$ (125.75 MHz, CD_2Cl_2, −80 °C): δ 127.84 (CH, central allylic), 113.04 (CH, C_5H_5), 100.61 (CH, terminal allylic), 77.26 (CH, terminal allylic), 66.16 (CH, bridgehead), 62.32 (CH, bridgehead), 46.39 (CH_3, Ti*Me*), 40.27 (CH_3, N*Me*), 37.74 (CH_2), 35.72 (CH_2), 27.93 (CH_3, Ti*Me*). Anal. Calcd for $C_{15}H_{23}NTi$: C, 67.92; H, 8.74; N, 5.28. Found: C, 67.54; H, 8.95; N, 5.17.

(Trop)$_2$ZrBn$_2$ (8). Complex **2** (103 mg; 0.254 mmol) was dissolved in THF (10 mL) and cooled to −30 °C. Benzylmagnesium chloride (1 M in ether; 0.48 mL; 0.48 mmol) was added to the solution and it was stirred at room temperature for 2 h. The solvents were removed in vacuo. Complex **8** was recovered by extraction of the residue with toluene. The volatile materials were removed to give 110 mg (88%) of an orange solid, which was recrystallized by vapor diffusion of pentane into a toluene solution of **8** at −30 °C to give analytically pure crystals. ^1H NMR (300 MHz, C_6D_6, RT): see Table 6. $^{13}C\{^1H\}$ NMR (100 MHz, C_6D_6, RT): δ 155.8 (C, ipso), 128.9 (CH, central allylic), 128.0 (CH, Ar), 125.7 (CH, Ar), 119.4 (CH, *p*-Ar), 83.8 (CH, terminal allylic), 66.4 (CH, bridgehead), 58.6 (CH_2Ar), 40.2 (N*Me*), 39.5 (CH_2). Anal. Calcd for $C_{30}H_{38}N_2Zr_1$: C, 69.58; H, 7.40; N, 5.41. Found: C, 69.56; H, 7.60; N, 5.21.

(Cp)(Trop)ZrBn$_2$ (9). Benzylmagnesium chloride (0.5 mL, 1.22 M) was added to a cooled (−30 °C) suspension of (Cp)(Trop)$ZrCl_2$ (0.106 g, 0.304 mmol) in Et_2O (8 mL). The reaction mixture was allowed to warm to room temperature and allowed to stir for 2 h. The orange supernatant was separated from $MgCl_2$ by filtration through Celite. The Et_2O was then removed under reduced pressure to leave an orange solid (0.132 g, 94% yield). Analytically pure material was obtained by slow cooling (−40 °C) of a saturated toluene solution. ^1H NMR (300 MHz, C_6D_6, 20 °C): see Table 6. $^{13}C\{^1H\}$ (125.75 MHz, C_6D_6, RT): δ 154.09 (C, ipso), 128.38 (CH, central allylic), 128.29 (CH, Ar), 128.30 (CH, Ar), 126.04 (CH, Ar), 120.43 (CH, *p*-Ar), 112.23 (CH, Cp), 81.72 (CH, terminal allylic), 66.54 (CH, bridgehead), 58.36 (CH_2), 39.65 (CH_3, N*Me*), 39.02 (CH_2, CH_2Ar). Anal. Calcd for $C_{27}H_{31}Cl_2NZr$: C, 70.38; H, 6.78; N, 3.01. Found: C, 70.02; H, 7.05; N, 3.05.

(Trop)$_2$Zr(Me)(O-*t*-Bu) (10). (Method A) From (Trop)$_2ZrMe_2$: Complex **5** (6.0 mg, 0.016 mmol) was dissolved in 4 mL of pentane and cooled to −30 °C, and *tert*-butyl alcohol (2.5 mg, 0.034 mmol) in pentane (2 mL) was added. The reaction mixture was stirred for 15 min. The volatile materials were removed under vacuum to yield (Trop)$_2$Zr(Me)(O-*t*-Bu) as an analytically pure pale yellow solid. (Method B) From (Trop)$_2$Zr(Me)(OSO_2CF_3): Potassium *tert*-butoxide (1.6 mg; 0.014 mmol) in THF (1 mL) was added to a solution of (Trop)$_2$Zr(Me)(OSO_2CF_3) (**11**) (67.0 mg, 0.013 mmol) in THF (2 mL) cooled to −30 °C. After 10 min at room temperature, the solvent was removed under reduced pressure, and the residue was extracted with pentane. The extracts were combined, and the solvent was removed in vacuo to give 5.0 mg (88%) of complex **5**. ^1H NMR (300 MHz, C_6D_6, 20 °C): δ 5.38 (t, J = 7.3 Hz, 2H, central allylic), 4.29 (m, 2H, terminal allylic), 4.02 (m, 2H, terminal allylic), 3.40 (m, 2H, bridgehead), 2.87 (m, 2H, bridgehead), 2.19 (m, 4H, CH_2), 1.86 (s, 10H, N*Me* and CH_2), 1.22 (s, 9H, O-*t*-*Bu*), 0.35 (s, 3H, Zr*Me*). $^{13}C\{^1H\}$ NMR (100 MHz, C_6D_6, 20 °C): δ 128.4 (CH, central allylic), 86.8 (CH, br, terminal allylic), 75.9 (C, CMe_3), 72.2 (CH, br, terminal allylic), 67.6 (CH, bridgehead), 65.5 (CH, bridgehead), 41.2 (CH_3, N*Me*), 39.8 (CH_2), 39.5 (CH_2), 33.0 (CMe_3), 10.0 (Zr*Me*). Anal. Calcd for $C_{21}H_{36}N_2O_1Zr_1$: C, 59.52; H, 8.56; N, 6.61. Found: C, 59.22; H, 8.74; N, 6.45.

(Trop)$_2$Zr(Me)(OSO_2CF_3) (11). Trifluoromethanesulfonic acid (9.8 μL, 0.11 mmol) was added to a solution of complex **5** (41.3 mg, 0.113 mmol) in pentane (12 mL) at −30 °C. The reaction mixture was warmed to room temperature and stirred for an additional 1 h. The volatile materials were removed in vacuo. The solid was washed with pentane (4 × 3 mL) until the filtrate was colorless. The residue was extracted with THF. The filtrate was collected and the solvent removed under reduced pressure to give 49.4 mg (89%) of yellow solid. Attempts to recrystallize **11** were unsuccessful, and substantial decomposition was observed when **11** was subjected to LRMS conditions. ^1H NMR (400 MHz, toluene-d_8, 20 °C): δ 5.11 (dd, J = 7.4 Hz, 2H, central allylic), 3.99 (m, 4H, terminal allylic), 3.12 (br s, 2H, bridgehead), 3.06 (br s, 2H, bridgehead), 1.92 (m, 4H, CH_2), 1.84 (s, 6H, N*Me*), 1.69 (m, 4H, CH_2), 0.38 (s, 3H, Zr*Me*). $^{13}C\{^1H\}$ NMR (100 MHz, toluene-d_8, 20 °C): δ 129.5, 128.6 (CH, central allylic), 85.3, 82.9 (CH, terminal allylic), 66.4, 66.0 (CH, bridgehead), 39.8 (CH_2), 39.1 (CH_3), 39.0 (CH_3) (CF_3 was not detected). $^{19}F\{^1H\}$ NMR (400 MHz, toluene-d_8, 20 °C): δ −77.0. LRMS (EI) m/z on $C_{18}H_{27}N_2F_3O_3SZr$ calcd: 498. Found: 499.

(Trop)$_2$Zr(Me)(NH-*t*-Bu) (12). A solution of complex **11** (44.1 mg, 0.0883 mmol) in THF (10 mL) was cooled to −30 °C, and LiNH-*t*-Bu (7.2 mg, 0.091 mmol) was added to it. The reaction mixture was warmed to room temperature and stirred for 15 min. The solvents were removed in vacuo and the residue extracted with toluene. The volatiles were removed under reduced pressure to give 34.2 mg (92%) of (Trop)$_2$Zr(Me)(NH-*t*-Bu). Attempts to recrystallize **12** were unsuccessful. Analysis by electron-impact mass spectrometry did not give satisfactory results, presumably due to decomposition of **12** under the experimental conditions. ^1H NMR (400 MHz, C_6D_6, 20 °C): δ 5.55 (t, J = 7.4 Hz, 2H, central allylic), 4.08 (m, 2H, terminal allylic), 3.81 (m, 2H, terminal allylic), 3.36 (br t, J = 5.3 Hz, 2H, bridgehead), 2.91 (br t, J = 5.4 Hz, 2H, bridgehead), 2.18 (m, 4H, CH_2), 1.92 (s, 6H, N*Me*), 1.88 (m, 4H, CH_2), 1.29 (s, 9H, *t*-*Bu*), −0.30 (s, 3H, Zr*Me*). ^1H NMR (300 MHz, THF-d_8, 20 °C): δ 5.48 (t, J = 7.4 Hz, 2 H, central allylic), 3.96 (m, 2H, terminal allylic), 3.88 (m, 2 H, terminal allylic), 3.86 (br s, 1H, N*H*), 3.22 (br s, 2 H, bridgehead), 3.23 (br s, 2 H, bridgehead), 2.20 (s, 6H, N*Me*), 2.19 (m, 8 H, CH_2), 1.08 (s, 9H, *t*-*Bu*), −0.17 (s, 3 H, Zr*Me*). $^{13}C\{^1H\}$ NMR (100 MHz, C_6D_6, 20 °C): δ 127.6 (CH, central allylic), 81.3 (CH, br, terminal allylic), 80.2 (C, CMe_3), 78.2 (CH, br, terminal allylic), 67.6 (CH, bridgehead), 66.1 (CH, bridgehead), 41.0 (CH_3, N*Me*), 39.6 (CH_2), 39.5 (CH_2), 34.9 (CH_3, CMe_3), 15.3 (CH_3, Zr*Me*).

(Cp)(Trop)Zr(CH_3)[N(2,6-$(CH_3)_2C_6H_2$)C(CH_3)] (13). A solution of 2,6-dimethylisocyanate (0.040 g, 0.30 mmol) in C_6H_6 (1 mL) was added to **6** (0.029 g, 0.30 mmol) in C_6H_6 (5 mL). The yellow color began to fade upon addition, and the reaction was allowed to proceed for 3 h. The solvent was removed under reduced pressure to give a yellow oil. The oil was extracted with pentane, and the combined extracts were cooled to −30 °C. After 2 days colorless blocks formed to give 0.092 g (70% yield) of analytically pure **13**. ^1H NMR (300 MHz, C_6D_6, 20 °C): δ 6.94 (3H, s, Ar*H*), 5.86 (5H, br, Cp*H*), 4.84 (1H, t, J = 7.2 Hz, central allylic), 3.80 (1H, br, terminal allylic), 3.51 (1H, br, bridgehead), 3.06 (1H, br, terminal allylic), 2.79 (1H, br, bridgehead), 2.09 (6H, s, Ar−CH_3) 1.96 (3H, s, N*Me*), 1.78 (3H, s, NC*Me*), 1.69 (4H, m, CH_2), 0.22 (3H, s, Zr*Me*). $^{13}C\{^1H\}$ (125.75 MHz, toluene-d_8, −50 °C): δ 247.59 (C, Zr*C*NAr), 147.50 (C, ipso), 130.46 (C, Ar), 129.72 (C, Ar), 128.37 (CH, Ar), 128.30 (CH, Ar), 127.11 (CH, br), 124.56 (CH), 106.83 (CH, Cp), 86.83 (CH, br), 68.04 (CH), 66.36 (CH), 65.09 (CH), 41.37 (CH_3, N*Me*), 39.63 (CH_2), 39.31 (CH_2), 23.18 (CH_3, CNCH_3), 19.01 (CH_3, ArCH_3), 18.95 (CH_3, CH_3Ar), 3.97 (CH_3, br, Zr*Me*). IR (KBr, cm^{-1}): 1577 (s, ν_{NC}). Anal. Calcd for $C_{24}H_{32}N_2Zr$: C, 65.55; H, 7.33; N, 6.37. Found: C, 65.39; H, 7.59; N, 6.04.

Catalyst Recovery Studies. A solution of (Cp)(Trop)$ZrCl_2$ (**3**) in toluene was added to a solution of MMAO to yield a solution 3.8×10^{-5} M in **3** and 0.04 M in MMAO. This solution was separated into three fractions. The first fraction was analyzed by UV−vis spectroscopy. The band at 421 nm (corresponding to **3**) was absent, indicating that all of **3** reacted with the MMAO. After several minutes the second fraction was quenched with solid (n-Bu)$_3$NHCl (to give a 0.4 M solution

in amine salt) and analyzed by UV−vis spectroscopy. Complex **3** was regenerated as evidenced by the reappearance of the band at 421 nm. From the absorbance of this band the concentration of **3** was calculated to be 4.4×10^{-5} M using the molar absorptivity ($\epsilon = 1.371$) obtained from a Beers law plot of **3** in pure toluene. The third fraction (5 mL) was placed under an atmosphere of ethylene. From the weight of PE generated the activity was calculated to be 2632×10^3 g PE/mol [Zr] h. A similar reaction sequence was performed in which 5 equiv of MMAO was added to 0.5 mL of orange solution (9.0×10^{-3} M) of **3** in toluene-d_8. The resulting red solution was quenched by adding 50 equiv of solid $(n\text{-Bu})_3$NHCl, and the original orange color was restored. Analysis of the quenched solution by NMR indicated 88% recovery of **3** relative to a ferrocene internal standard.

Generation of [(Cp)(Trop)Zr(CH$_3$)][CH$_3$B(C$_6$F$_5$)$_3$] (14). Cooled (−30 °C) C_6D_5Cl (0.4 mL) was added to 2.5 mg (0.0081 mmol) of **6** and 4.1 mg (0.0081 mmol) of $B(C_6F_5)_3$ at −30 °C. The solution was mixed, placed in a NMR tube, sealed with a Teflon valve, removed from the glovebox, and immediately cooled to −196 °C. The sample was then placed in a precooled NMR spectrometer probe, warmed to the desired temperature, and characterized by NMR spectroscopy. ^{1}H NMR (500 MHz, C_6D_5Cl, 0 °C): δ 5.95 (5H, br, C_5H_5), 4.89 (1H, br, central allylic), 4.16 (2H, br, terminal allylic), 2.69 (2H, br, bridgehead), 1.86 (2H, br, CH_2), 1.64 (2H, br, CH_2), 1.58 (3H, br, NCH_3), 0.627 (3H, br, BCH_3), 0.18 (3H, br, $ZrCH_3$). ^{11}B NMR (160 MHz, C_6D_5Cl, 0 °C): δ −15.1 (s, $MeB(C_6F_5)_3$). ^{19}F NMR (400 MHz, C_6D_5Cl, RT): δ 132.9 (d, $J_{FF} = 40$ Hz, 2 F, *o*-F), 160.4 (br, 1 F, *p*-F), 154.7 (br, 2 F, *m*-F).

X-ray Crystal Structure of (Trop)$_2$ZrCl$_2$ (2). An orange platelike crystal was grown by slow cooling of a saturated CH_2Cl_2 solution and mounted on a glass fiber using Paratone N hydrocarbon oil. All measurements were made on a Siemens SMART (Siemens Industrial Automation, Inc.) diffractometer with a CCD area detector with graphite-monochromated Mo Kα radiation ($\lambda = 0.71069$ Å).

Cell constants and an orientation matrix were obtained from a least-squares refinement using the measured positions of 4979 reflections in the range $3.00° < 2\theta < 45.00°$ and corresponded to a primitive orthorhombic cell with dimensions given in Table 1. On the basis of systematic absences, packing considerations, a statistical analysis of intensity distribution, and successful solution and refinement of the structure, the space group was determined to be $P2_1/n$ (#14). Frames corresponding to an arbitrary hemisphere of data were collected using ω scans of 0.3° counted for a total of 10.0 s per frame.

Data were integrated by the program SAINT (Siemens Industrial Automation, Inc.) to a maximum 2θ value given in Table 1. The data were corrected for Lorentz and polarization effects. Data were analyzed for agreement and possible absorption using XPREP (Siemens Industrial Automation, Inc.). An empirical absorption correction based on comparison of redundant and equivalent reflections was applied using XPREP ($T_{max} = 0.91$, $T_{min} = 0.80$).

The structure was solved by direct methods[109] and expanded using Fourier techniques. Non-hydrogen atoms were refined anisotropically. Hydrogen atoms were refined isotropically. The final cycle of full-matrix least-squares refinement, based on the observed reflections and variable parameters given in the Supporting Information, converged with unweighted and weighted agreement factors (R and R_w, respectively) given in Table 1.

Neutral atom scattering factors were taken from Cromer and Waber.[110] Anomalous dispersion effects were included in F_{calc};[111] the values for $\Delta f'$ and $\Delta f''$ were those of Creagh and McAuley.[112] The values for the mass attenuation coefficients are those of Creagh and Hubble.[113] All calculations were performed using the teXsan crystallographic software package of the Molecular Structure Corporation. An ORTEP diagram is given in Figure 1; selected bond lengths and angles are given in Table 2. A complete listing of experimental details, positional and anisotropic thermal parameters, and tables of bond lengths and bond angles are provided as Supporting Information for all compounds characterized by X-ray crystallography.

X-ray Crystal Structure of (Cp)(Trop)ZrCl$_2$ (3). An orange columnar crystal of **3**, grown from slow cooling of a saturated CH_2Cl_2 solution at −30 °C, was mounted on a glass fiber using Paratone N hydrocarbon oil.

Cell constants and an orientation matrix, obtained from a least-squares refinement using the measured positions of 2890 reflections in the range $3.00° < 2\theta < 45.00°$, corresponded to a primitive orthorhombic cell with dimensions given in Table 1. On the basis of the systematic absences, packing considerations, a statistical analysis of intensity distribution, and successful solution and refinement of the structure, the space group was determined to be *Pnma* (#62). Data reduction and structure solution and refinement were performed as described for **2**. An ORTEP diagram is given in Figure 2; selected bond lengths and angles are given in Table 3.

X-ray Crystal Structure of (Trop)$_2$ZrBn$_2$ (8). X-ray quality crystals were obtained by slow cooling of a pentane solution at −30 °C. The crystal mounting, data collection, data reduction, and solution and refinement were performed as described for the X-ray crystallographic analysis of **2** except the cell constants were determined using 8192 reflections. An ORTEP diagram is given in Figure 3; selected bond lengths and angles are given in Table 5.

X-ray Crystal Structure of (Cp)(Trop)Zr(CH$_3$)[N(2,6-(CH$_3$)$_2$C$_6$H$_2$)C(CH$_3$)] (13). A single colorless prismatic crystal, grown from slow cooling of a saturated pentane solution at −30 °C, was analyzed by X-ray crystallography. The crystal mounting, data collection, data reduction, and the solution and refinement were performed as described for the X-ray crystallographic analysis of **2** except the cell constants were determined using 7082 reflections. An ORTEP diagram is given in Figure 7; selected bond lengths and angles are given in Table 9.

Acknowledgment. We thank the Union Carbide Corporation, South Charleston, WV, for GPC data, Albermarle Corporation (Dr. Bruce Berris) for a gift of tris(pentafluorophenyl)borane, and Kyle Fujdala and Professor T. Don Tilley for DSC data. We also acknowledge Drs. Dana Caulder and Ryan Powers, University of California, Berkeley, X-ray diffraction facility (CHEXRAY), for assistance with the X-ray studies. C.M. is grateful for a postdoctoral fellowship from the Spanish Ministry of Education and Culture. We are grateful for support of this work from the National Science Foundation (Grant No. CHE-9633374).

Supporting Information Available: Tables of crystal data, ORTEP diagrams, bond distances and angles, and positional and displacement parameters for complexes **2**, **3**, **5**, **8**, and **13** and spectroscopic data for **6** and **4a/4b** are provided. This material is available free of charge via the Internet at http://pubs.acs.org.

OM000038K

(109) Altomare, A.; Camalli, M.; Cascarano, M.; Giacovazzo, C.; Guagliardi, A. *J. Appl. Crystallogr.* **1993**, *26*, 343.
(110) Cromer, D. T.; Waber, J. T. *International Tables for X-ray Crystallography*; Kynoch Press: Birmingham, England, 1974; Vol. IV, pp 72−94.
(111) Ibers, J. A.; Hamilton, W. C. *Acta Crystallogr.* **1964**, *17*, 781.
(112) Creagh, D. C.; McAuley, W. J. *International Tables for Crystallography*; Wilson, A. J. C., Ed.; Kluwer Academic Publishers: Boston, 1992; Vol. C, pp 219−222.
(113) Creagh, D. C.; Hubble, J. H. *International Tables for Crystallography*; Wilson, A. J. C., Ed.; Kluwer Academic Publishers: Boston, 1992; Vol. C, pp 200−206.